that there was direct contact between the microglia/macrophages and synaptic structures, immune-electron microscopic examination was performed. Consistent with the confocal imaging, this analysis showed that the microglia/macrophages made direct contact with both presynaptic and postsynaptic structures (Figure 6B). These observations indicated that classically activated microglia/macrophages had migrated to the compressed spinal cord and eliminated synaptic terminals.

Discussion

In the present study, we showed that severe chronic progressive spinal cord compression in *twy* mice caused more body weight loss and neurological deficits in motor function than milder spinal cord progression. Furthermore, M1 macrophage-dominant inflammation was present in mice with a severely compressed spinal cord. In agreement, Cyr61, an inducer of M1 macrophages, was also markedly upregulated in these spinal cords. Furthermore, immunostaining and electron microscopic analyses indicated that the inflammatory C1q complement cascade eliminated synapse formation, resulting in neurodegeneration.

Macrophages are typically divided into classically activated (M1) and alternatively activated (M2) macrophages [32]. M1 macrophages, activated via TLRs, produce proinflammatory cytokines and oxidative metabolites [33]. Here we found that the M1 macrophage and TLR signals were activated in the chronically compressed spinal cord. These results were consistent with the distribution of M1 macrophages in traumatic spinal cord injury that continues even during the chronic phase [34,35]. The shift to M1 macrophages, which have deleterious and cytotoxic effects [36], may represent the main pathology of the neurodegeneration that accompanies chronic spinal cord compression.

Although the extracellular matrix has been classically viewed as an inert scaffold, recent studies have revealed that it influences diverse aspects of cellular behavior and function [37]. Cyr61 is a matricellular protein that is highly expressed at sites of inflammation, where its ability to regulate gene expression in macrophages plays an important role [25,38]. In addition, various mechanical stresses induce Cyr61 expression in cartilage/bone tissues and periodontal ligaments [26,39]. Our present data indicated that Cyr61 is significantly upregulated in the chronically, severely compressed spinal cord and colocalizes extensively with reactive astrocytes. These findings suggest that Cyr61 engages in a distinct intracellular signaling cascade in microglia/macrophages and promotes M1 macrophage recruitment in the compressed spinal cord.

Microglia/macrophages were recently identified as the phagocytes responsible for eliminating tagged synapses, via classical complement signaling [40], and the complement cascade is strongly induced in the brain tissues of patients with various neurodegenerative diseases [41]. Interestingly, in a mouse model of glaucoma, a relatively common neurodegenerative disease related to high intraocular pressure, the classical complement pathway is upregulated long before retinal ganglion cell death occurs [28]. Yet another study suggested that initiation of the classical complement pathway via C1q is detrimental to recovery after spinal cord injury [42]. The present microarray and immunohistochemical analyses showed that the classical complement pathway via C1q was significantly upregulated in the severely compressed spinal cord. Our findings raise the intriguing possibility that Clq may also be involved in synapse elimination in the chronically compressed spinal cord. Future studies should examine whether the inhibition of C1q in animal models of chronic spinal cord compression hinders the associated neurodegenerative changes.

Previous studies on the surgical outcomes of CCM patients demonstrated that the postoperative recovery was poor in those with severe canal stenosis, because irreversible changes had occurred in the spinal cord [5]. Recent studies have revealed that neural stem cell therapy can be an effective treatment for previously incurable nervous system disorders, such as spinal cord injury [43-47]. Therefore, an appropriate stem cell treatment for CCM should be examined in future studies.

To our knowledge, these data are the first to document the detailed pathophysiology of the inflammatory response in an animal model of chronic spinal cord compression. The clinical implications are noteworthy, because manipulation of the classical complement cascade in the chronically compressed spinal cord could be a strategy for minimizing synapse loss and secondary neurodegeneration due to inflammation. We believe that our findings are valuable for future research on the alterations taking place in the inflammatory environment in CCM.

Abbreviations

CCM: cervical compressive myelopathy; Cyr61: cysteine-rich protein 61; FOV: field of view; RT-PCR: reverse transcriptase polymerase chain reaction; TLR: toll-like receptor; *twy*: tip-toe walking Yoshimura.

Competing interests

H. Okano is the scientific consultant of San Bio, Inc; Eisai Co Ltd; and Daiichi Sankyo Co Ltd. The remaining authors declare that they have no competing interests.

Authors' contributions

MT, HO, and MN conceived and designed the experiments. MT, SK, YK, SS, and KH performed the experiments. MT, SK, and SS analyzed the data. YT, HO, and MN contributed the reagents, materials, and analysis tools. MT, HO, and MN wrote the paper. All authors read and approved the final manuscript.

Acknowledgements

This work was supported by grants from the Japan Science and Technology-California Institute for Regenerative Medicine collaborative program; a medical research grant on traffic accidents from the General Insurance Association of Japan; and a Grant-in-Aid for the Global COE program from MEXT to Keio University. We thank A. Iwanami, T. Konomi, Y. Kobayashi, S. Nishimura, and H. Iwai for their advice on the experimental approach. We thank C. Yamada for tender animal care and technical support.

Author details
[1]Department of Orthopedic Surgery, Keio University School of Medicine, 35 Shinanomachi, Shinjuku-ku, Tokyo 160-8582, Japan. [2]Department of Physiology, Keio University School of Medicine, 35 Shinanomachi, Shinjuku-ku, Tokyo 160-8582, Japan. [3]Central Institute for Experimental Animals, 3-25-12 Tonomachi, Kawasakiku, Kawasaki, Kanagawa 210-0821, Japan.

Received: 5 January 2014 Accepted: 17 February 2014
Published: 4 March 2014

References

1. Bohlman HH, Emery SE: The pathophysiology of cervical spondylosis and myelopathy. *Spine (Phila Pa 1976)* 1988, 13:843–846.
2. Fehlings MG, Skaf G: A review of the pathophysiology of cervical spondylotic myelopathy with insights for potential novel mechanisms drawn from traumatic spinal cord injury. *Spine (Phila Pa 1976)* 1998, 23:2730–2737.
3. Kameyama T, Hashizume Y, Ando T, Takahashi A, Yanagi T, Mizuno J: Spinal cord morphology and pathology in ossification of the posterior longitudinal ligament. *Brain* 1995, 118:263–278.
4. Mizuno J, Nakagawa H, Chang HS, Hashizume Y: Postmortem study of the spinal cord showing snake-eyes appearance due to damage by ossification of the posterior longitudinal ligament and kyphotic deformity. *Spinal Cord* 2005, 43:503–507.
5. Baba H, Imura S, Kawahara N, Nagata S, Tomita K: Osteoplastic laminoplasty for cervical myeloradiculopathy secondary to ossification of the posterior longitudinal ligament. *Int Orthop* 1995, 19:40–45.
6. Iwasaki M, Okuda S, Miyauchi A, Sakaura H, Mukai Y, Yonenobu K, Yoshikawa H: Surgical strategy for cervical myelopathy due to ossification of the posterior longitudinal ligament: part 1: clinical results and limitations of laminoplasty. *Spine (Phila Pa 1976)* 2007, 32:647–653.
7. Okawa A, Nakamura I, Goto S, Moriya H, Nakamura Y, Ikegawa S: Mutation in Npps in a mouse model of ossification of the posterior longitudinal ligament of the spine. *Nat Genet* 1998, 19:271–273.
8. Uchida K, Baba H, Maezawa Y, Kubota C: Progressive changes in neurofilament proteins and growth-associated protein-43 immunoreactivities at the site of cervical spinal cord compression in spinal hyperostotic mice. *Spine (Phila Pa 1976)* 2002, 27:480–486.
9. Yamaura I, Yone K, Nakahara S, Nagamine T, Baba H, Uchida K, Komiya S: Mechanism of destructive pathologic changes in the spinal cord under chronic mechanical compression. *Spine (Phila Pa 1976)* 2002, 27:21–26.
10. Takano M, Komaki Y, Hikishima K, Konomi T, Fujiyoshi K, Tsuji O, Toyama Y, Okano H, Nakamura M: In vivo tracing of neural tracts in tiptoe walking Yoshimura mice by diffusion tensor tractography. *Spine (Phila Pa 1976)* 2013, 38:E66–E72.
11. Yu WR, Baptiste DC, Liu T, Odrobina E, Stanisz GJ, Fehlings MG: Molecular mechanisms of spinal cord dysfunction and cell death in the spinal hyperostotic mouse: implications for the pathophysiology of human cervical spondylotic myelopathy. *Neurobiol Dis* 2009, 33:149–163.
12. Yato Y, Fujimura Y, Nakamura M, Watanabe M, Yabe Y: Decreased choline acetyltransferase activity in the murine spinal cord motoneurons under chronic mechanical compression. *Spinal Cord* 1997, 35:729–734.
13. Yu WR, Liu T, Kiehl TR, Fehlings MG: Human neuropathological and animal model evidence supporting a role for Fas-mediated apoptosis and inflammation in cervical spondylotic myelopathy. *Brain* 2011, 134:1277–1292.
14. Uchida K, Baba H, Maezawa Y, Furukawa S, Furusawa N, Imura S: Histological investigation of spinal cord lesions in the spinal hyperostotic mouse (twy/twy): morphological changes in anterior horn cells and immunoreactivity to neurotropic factors. *J Neurol* 1998, 245:781–793.
15. Baltes C, Radzwill N, Bosshard S, Marek D, Rudin M: Micro MRI of the mouse brain using a novel 400 MHz cryogenic quadrature RF probe. *NMR Biomed* 2009, 22:834–842.
16. Bosshard SC, Baltes C, Wyss MT, Mueggler T, Weber B, Rudin M: Assessment of brain responses to innocuous and noxious electrical forepaw stimulation in mice using BOLD fMRI. *Pain* 2010, 151:655–663.
17. Baba H, Furusawa N, Fukuda M, Maezawa Y, Imura S, Kawahara N, Nakahashi K, Tomita K: Potential role of streptozotocin in enhancing ossification of the posterior longitudinal ligament of the cervical spine in the hereditary spinal hyperostotic mouse (twy/twy). *Eur J Histochem* 1997, 41:191–202.
18. Takano M, Hikishima K, Fujiyoshi K, Shibata S, Yasuda A, Konomi T, Hayashi A, Baba H, Honke K, Toyama Y, Okano H, Nakamura M: MRI characterization of paranodal junction failure and related spinal cord changes in mice. *PLoS One* 2012, 7:e52904.
19. Ogura H, Matsumoto M, Mikoshiba K: Motor discoordination in mutant mice heterozygous for the type 1 inositol 1,4,5-trisphosphate receptor. *Behav Brain Res* 2001, 122:215–219.
20. Mistry DS, Chen Y, Sen GL: Progenitor function in self-renewing human epidermis is maintained by the exosome. *Cell Stem Cell* 2012, 11:127–135.
21. Kigerl KA, Lai W, Rivest S, Hart RP, Satoskar AR, Popovich PG: Toll-like receptor (TLR)-2 and TLR-4 regulate inflammation, gliosis, and myelin sparing after spinal cord injury. *J Neurochem* 2007, 102:37–50.
22. Long HQ, Li GS, Hu Y, Wen CY, Xie WH: HIF-1alpha/VEGF signaling pathway may play a dual role in secondary pathogenesis of cervical myelopathy. *Med Hypotheses* 2012, 79:82–84.
23. Kele J, Simplicio N, Ferri AL, Mira H, Guillemot F, Arenas E, Ang SL: Neurogenin 2 is required for the development of ventral midbrain dopaminergic neurons. *Development* 2006, 133:495–505.
24. Tanabe F, Yone K, Kawabata N, Sakakima H, Matsuda F, Ishidou Y, Maeda S, Abematsu M, Komiya S, Setoguchi T: Accumulation of p62 in degenerated spinal cord under chronic mechanical compression: functional analysis of p62 and autophagy in hypoxic neuronal cells. *Autophagy* 2011, 7:1462–1471.
25. Bai T, Chen CC, Lau LF: Matricellular protein CCN1 activates a proinflammatory genetic program in murine macrophages. *J Immunol* 2010, 184:3223–3232.
26. Chaqour B, Goppelt-Struebe M: Mechanical regulation of the Cyr61/CCN1 and CTGF/CCN2 proteins. *FEBS J* 2006, 273:3639–3649.
27. Kivela R, Kyrolainen H, Selanne H, Komi PV, Kainulainen H, Vihko V: A single bout of exercise with high mechanical loading induces the expression of Cyr61/CCN1 and CTGF/CCN2 in human skeletal muscle. *J Appl Physiol* 2007, 103:1395–1401.
28. Stevens B, Allen NJ, Vazquez LE, Howell GR, Christopherson KS, Nouri N, Micheva KD, Mehalow AK, Huberman AD, Stafford B, Sher A, Litke AM, Lambris JD, Smith SJ, John SW, Barres BA: The classical complement cascade mediates CNS synapse elimination. *Cell* 2007, 131:1164–1178.
29. Zhang Z, Pinto AM, Wan L, Wang W, Berg MG, Oliva I, Singh LN, Dengler C, Wei Z, Dreyfuss G: Dysregulation of synaptogenesis genes antecedes motor neuron pathology in spinal muscular atrophy. *Proc Natl Acad Sci U S A* 2013, 110:19348–19353.
30. Stephan AH, Madison DV, Mateos JM, Fraser DA, Lovelett EA, Coutellier L, Kim L, Tsai HH, Huang EJ, Rowitch DH, Berns DS, Tenner AJ, Shamloo M, Barres BA: A dramatic increase of C1q protein in the CNS during normal aging. *J Neurosci* 2013, 33:13460–13474.
31. Naito AT, Sumida T, Nomura S, Liu ML, Higo T, Nakagawa A, Okada K, Sakai T, Hashimoto A, Hara Y, Shimizu I, Zhu W, Toko H, Katada A, Akazawa H, Oka T, Lee JK, Minamino T, Nagai T, Walsh K, Kikuchi A, Matsumoto M, Botto M, Shiojima I, Komuro I: Complement C1q activates canonical Wnt signaling and promotes aging-related phenotypes. *Cell* 2012, 149:1298–1313.
32. Gordon S: Alternative activation of macrophages. *Nat Rev Immunol* 2003, 3:23–35.
33. Mantovani A, Sica A, Sozzani S, Allavena P, Vecchi A, Locati M: The chemokine system in diverse forms of macrophage activation and polarization. *Trends Immunol* 2004, 25:677–686.
34. Kigerl KA, Gensel JC, Ankeny DP, Alexander JK, Donnelly DJ, Popovich PG: Identification of two distinct macrophage subsets with divergent effects causing either neurotoxicity or regeneration in the injured mouse spinal cord. *J Neurosci* 2009, 29:13435–13444.
35. Guerrero AR, Uchida K, Nakajima H, Watanabe S, Nakamura M, Johnson WE, Baba H: Blockade of interleukin-6 signaling inhibits the classic pathway and promotes an alternative pathway of macrophage activation after spinal cord injury in mice. *J Neuroinflammation* 2012, 9:40.
36. Laskin DL: Macrophages and inflammatory mediators in chemical toxicity: a battle of forces. *Chem Res Toxicol* 2009, 22:1376–1385.
37. Aszodi A, Legate KR, Nakchbandi I, Fassler R: What mouse mutants teach us about extracellular matrix function. *Annu Rev Cell Dev Biol* 2006, 22:591–621.
38. Jun JI, Lau LF: The matricellular protein CCN1 induces fibroblast senescence and restricts fibrosis in cutaneous wound healing. *Nat Cell Biol* 2010, 12:676–685.
39. Li Y, Li M, Tan L, Huang S, Zhao L, Tang T, Liu J, Zhao Z: Analysis of time-course gene expression profiles of a periodontal ligament tissue model under compression. *Arch Oral Biol* 2012, 58:511–522.

40. Aguzzi A, Barres BA, Bennett ML: **Microglia: scapegoat, saboteur, or something else?** *Science* 2013, **339**:156–161.
41. Stephan AH, Barres BA, Stevens B: **The complement system: an unexpected role in synaptic pruning during development and disease.** *Annu Rev Neurosci* 2012, **35**:369–389.
42. Galvan MD, Luchetti S, Burgos AM, Nguyen HX, Hooshmand MJ, Hamers FP, Anderson AJ: **Deficiency in complement C1q improves histological and functional locomotor outcome after spinal cord injury.** *J Neurosci* 2008, **28**:13876–13888.
43. Amoh Y, Li L, Campillo R, Kawahara K, Katsuoka K, Penman S, Hoffman RM: **Implanted hair follicle stem cells form Schwann cells that support repair of severed peripheral nerves.** *Proc Natl Acad Sci U S A* 2005, **102**:17734–17738.
44. Amoh Y, Li L, Katsuoka K, Hoffman RM: **Multipotent hair follicle stem cells promote repair of spinal cord injury and recovery of walking function.** *Cell Cycle* 1865–1869, **2008**:7.
45. Amoh Y, Li L, Katsuoka K, Penman S, Hoffman RM: **Multipotent nestin-positive, keratin-negative hair-follicle bulge stem cells can form neurons.** *Proc Natl Acad Sci U S A* 2005, **102**:5530–5534.
46. Li L, Mignone J, Yang M, Matic M, Penman S, Enikolopov G, Hoffman RM: **Nestin expression in hair follicle sheath progenitor cells.** *Proc Natl Acad Sci U S A* 2003, **100**:9958–9961.
47. Liu F, Uchugonova A, Kimura H, Zhang C, Zhao M, Zhang L, Koenig K, Duong J, Aki R, Saito N, Mii S, Amoh Y, Katsuoka K, Hoffman RM: **The bulge area is the major hair follicle source of nestin-expressing pluripotent stem cells which can repair the spinal cord compared to the dermal papilla.** *Cell Cycle* 2011, **10**:830–839.

doi:10.1186/1742-2094-11-40
Cite this article as: Takano *et al.*: Inflammatory cascades mediate synapse elimination in spinal cord compression. *Journal of Neuroinflammation* 2014 **11**:40.

Zhang et al. Molecular Brain 2014, 7:14
http://www.molecularbrain.com/content/7/1/14

Molecular Brain

RESEARCH Open Access

Rewiring of regenerated axons by combining treadmill training with semaphorin3A inhibition

Liang Zhang[1,2,3†], Shinjiro Kaneko[1,4†], Kaoru Kikuchi[5], Akihiko Sano[5], Miho Maeda[5], Akiyoshi Kishino[5], Shinsuke Shibata[2], Masahiko Mukaino[3], Yoshiaki Toyama[1], Meigen Liu[3], Toru Kimura[5], Hideyuki Okano[2*†] and Masaya Nakamura[1*†]

Abstract

Background: Rats exhibit extremely limited motor function recovery after total transection of the spinal cord (SCT). We previously reported that SM-216289, a semaphorin3A inhibitor, enhanced axon regeneration and motor function recovery in SCT adult rats. However, these effects were limited because most regenerated axons likely do not connect to the right targets. Thus, rebuilding the appropriate connections for regenerated axons may enhance recovery. In this study, we combined semaphorin3A inhibitor treatment with extensive treadmill training to determine whether combined treatment would further enhance the "rewiring" of regenerated axons. In this study, which aimed for clinical applicability, we administered a newly developed, potent semaphorin3A inhibitor, SM-345431 (Vinaxanthone), using a novel drug delivery system that enables continuous drug delivery over the period of the experiment.

Results: Treatment with SM-345431 using this delivery system enhanced axon regeneration and produced significant, but limited, hindlimb motor function recovery. Although extensive treadmill training combined with SM-345431 administration did not further improve axon regeneration, hindlimb motor performance was restored, as evidenced by the significant improvement in the execution of plantar steps on a treadmill. In contrast, control SCT rats could not execute plantar steps at any point during the experimental period. Further analyses suggested that this strategy reinforced the wiring of central pattern generators in lumbar spinal circuits, which, in turn, led to enhanced motor function recovery (especially in extensor muscles).

Conclusions: This study highlights the importance of combining treatments that promote axon regeneration with specific and appropriate rehabilitations that promote rewiring for the treatment of spinal cord injury.

Keywords: Axonal regeneration, Semaphorin3A, Inhibitor, Rehabilitation, Rewiring, Drug delivery system

Background

Severe spinal cord injuries (SCI) in adult mammals result in various deficits throughout life. The limited capability of axons to regenerate in the central nervous system (CNS) is thought to be the main reason for these lasting deficits. Previous studies have suggested that both extrinsic and intrinsic factors in the CNS contribute to this incapacity for axonal regeneration [1-4]. Several distinct extrinsic molecules have been proposed to hinder axonal regeneration, including CNS myelin-associated proteins (MAG, Nogo, OMgp) [5-9], chondroitin sulphate proteoglycans [10,11], semaphorin3A [12,13] and RGM (repulsive guidance molecule) [14,15]. Neutralizing one (or several) of these molecules enhances axonal regeneration and results in some degree of functional recovery [10,16,17]. Until recently, it remained unknown whether neutralizing semaphorin3A would also lead to axonal regeneration and motor function recovery, in part because semaphorin3A deficiency is lethal [18]. Thus, we previously developed a selective and potent semaphorin3A inhibitor called SM-216289 [19] that selectively inhibits semaphorin3A signaling both *in vitro* and *in vivo* [20]. Administration of SM-216289 to adult rats after total spinal cord transection

* Correspondence: hidokano@a2.keio.jp; masa@a8.keio.jp
†Equal contributors
[2]Department of Physiology, Keio University School of Medicine, 35 Shinanomachi, Shinjuku, Tokyo 160-8582, Japan
[1]Department of Orthopedic Surgery, Keio University School of Medicine, 35 Shinanomachi, Shinjuku, Tokyo 160-8582, Japan
Full list of author information is available at the end of the article

(SCT) led to axonal regeneration and motor function recovery [20]. In addition, axonal regeneration and functional recovery have now been observed after several treatments that block 1 or more axonal growth inhibitors (including SM-216289). However, these effects are moderate at best, presumably because most of the regenerated axons do not connect with the correct targets [21]. Thus, rebuilding the appropriate connections of regenerated axons in lesioned spinal cords remains an important unresolved issue.

Body weight-supported treadmill training induces plastic changes in lesioned spinal cords and is useful for maximizing residual locomotor function after moderate SCI [22,23]. Furthermore, even after severe SCI, treadmill training partially improves hindlimb coordination [24] by inducing plasticity in specific spinal locomotor circuits called "central pattern generators" (CPGs). More specifically, these plastic changes have been shown to result in the recovery of plantar step walking in cats [25] and neonatal rats [26]. Furthermore, SCT adult rats partially recover plantar step walking when treadmill training is combined with other appropriate treatments, such as epidural electrical stimulation [27], pharmacological treatments [24] or cell transplantation [28]. Thus, with specific and appropriate rehabilitation, spinal cord CPGs can be reorganized, and functionally appropriate connections between CPGs and regenerated (or residual) axons can be rebuilt. Therefore, we hypothesized that extensive treadmill training would assist in the correct wiring of axons regenerated by semaphorin3A inhibitor treatment and that this rewiring may contribute to further motor functional recovery after SCT.

However, several issues, including drug delivery, remain to be resolved before semaphorin3A inhibitors can be used in the clinic. In an attempt to resolve these issues, we developed a novel selective semaphorin3A inhibitor, SM-345431 (Vinaxanthone), which demonstrates physicochemical properties equivalent to those of SM-216289 but also improvements that should allow for the development of a higher quality pharmaceutical product. Additionally, we developed a novel drug delivery system (DDS) utilizing a silicone sheet. With future clinical applications in mind, we chose to evaluate SM-345431 with this novel DDS. We observed that, consistent with our previous study [20], SM-345431 treatment enhanced axon regeneration and resulted in significant, but limited, hindlimb motor function recovery. Although extensive treadmill training with SM-345431 administration did not further improve axon regeneration, hindlimb motor performance was restored, as evidenced by the execution of plantar steps on a treadmill using a body support system (BSS). Moreover, immunohistological analysis suggested that SM-345431 administration with treadmill training reinforced the wiring of CPGs in lumbar spinal circuits and led to enhanced motor function recovery, especially in extensor muscles.

Results

Evaluation of a novel DDS and the activity of SM-345431 *in vitro*

In our previous study, we used an osmotic mini-pump to deliver the semaphorin3A inhibitor SM-216289 [20]. However, in clinical practice, this type of invasive drug delivery method is not ideal. Therefore, we developed a novel DDS that utilizes a silicone matrix to continuously deliver SM-345431 (a newly developed semaphorin3A inhibitor) intrathecally. We evaluated the drug release profile of SM-345431 in this new silicone matrix preparation and the potency of SM-345431-mediated semaphorin3A inhibition in vitro (Figure 1). SM-345431 exhibited semaphorin3A inhibiting activity with an IC50 of 0.1-0.2 μM in growth cone collapse assays using E8 chick and E14 rat dorsal root ganglia (DRG) (Figure 1A). When chick embryonic DRG explants and semaphorin3A-expressing COS7 cell aggregates (semaphorin3A-COS) were co-cultured in a collagen gel, the neurites of the DRG explants grew away from the semaphorin3A-COS, as shown in Figure 1B. However, when DRG explants and semaphorin3A-COS were co-cultured in the presence of SM-345431, radial extensions of the neurites were observed, which suggests that the chemo-repulsive effects of semaphorin3A were blocked by SM-345431 in a dose-dependent manner (Figure 1B). We also evaluated the selectivity of SM-345431 for semaphorin3A inhibition by examining the pharmacological profile of SM-345431 (Tables 1 and 2). As shown in these tables, the IC50 value for semaphorin3A inhibition was substantially lower than the other IC50s, which suggested that SM-345431 is a highly selective semaphorin3A inhibitor. To examine the semaphorin3A inhibiting activity of SM-345431 while it was being released from the silicone matrix (SM-345431-silicone), 1 mg of a silicone sheet containing 100 μg SM-345431 was placed into collagen gel cultures containing DRG explants and semaphorin3A-COS (Figure 1C). Assuming that 5% of the SM-345431 was released and uniformly diffused throughout the culture during the 2 days of incubation, the final concentration of SM-345431 was approximately 5 μM, which is a large enough dose to inhibit semaphorin3A activity. Radial neurite extension was observed in cultures with SM-345431-silicone but not in those with control silicone, indicating that semaphorin3A activity had been inhibited by SM-345431. We also measured the cumulative percentage of released doses of SM-345431 using this DDS over 2 months *in vitro* (Figure 1E) and found that this DDS released a constant dose of SM-345431 and was stable *in vitro*. When 7 mm × 5 mm × 0.3 mm sheets were used, the amount of drug release stabilized at approximately 10 μg/day after an initial peak of drug release that occurred over the first 2 days (Figure 1F). For the *in vivo* study, we trimmed the silicone sheet into 3 mm × 3 mm × 0.3 mm pieces to fit the injury site following SCT (Figure 1G-I).

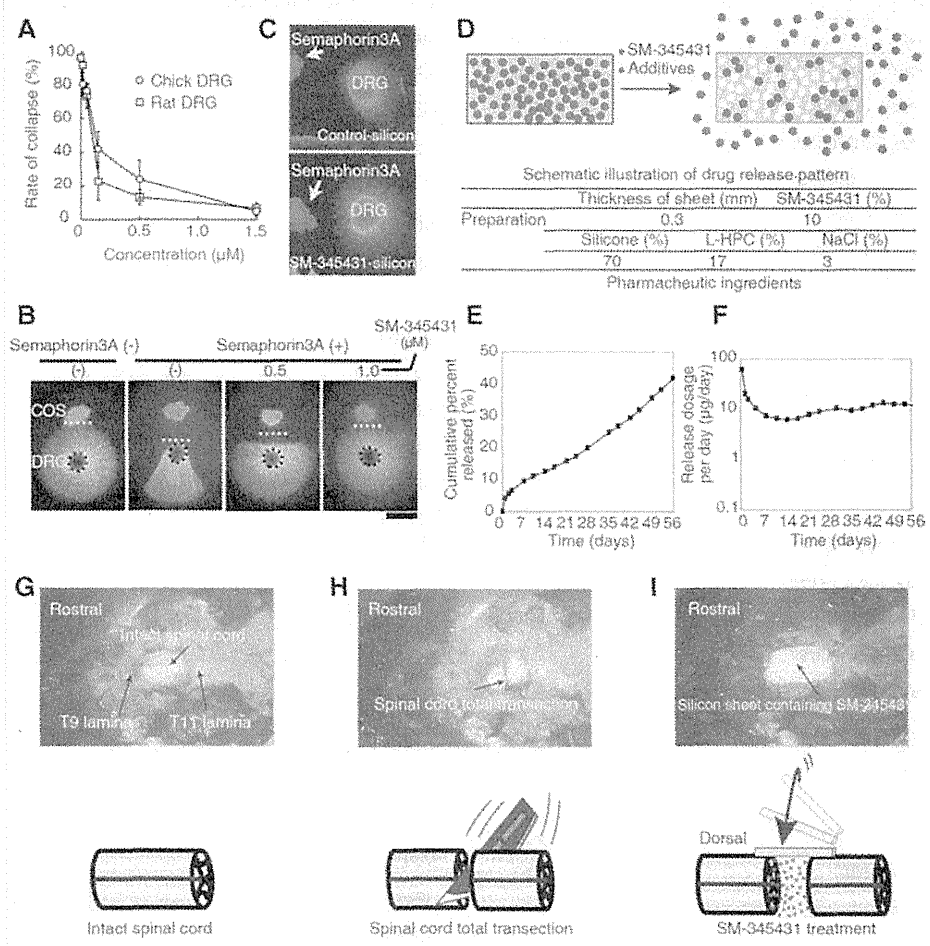

Figure 1 Preparation of the SM-345431 silicone DDS and *in vitro* release study. **(A)** Analysis of the inhibitory activity of SM-345431 in the growth cone collapse assay using E8 chick and E14 rat DRGs. **(B)** Collagen co-culture assay using E8 chick DRGs and semaphorin3A-expressing COS7 cell aggregates. **(C)** Pictures showing the effects of SM-345431-silicone or control-silicone in the collagen gel. **(D)** Schematic illustration of drug release from the matrix silicone preparation; the drug is dissolved in water, permeates into the preparation and is then released. The rate of water permeation into the silicone matrix is controlled by various additives, and the proportions of these additives included in the DDS control the variations in the drug release profile. The preparation used here contained the water-soluble additives listed in the table **(D)**. Stable and linear release of SM-345431 was observed for up to 2 months as shown in **(E)** and **(F)**. **(E, F)** SM-345431 release curve for the preparation. The linear cumulative percent release curve at 2 months **(E)** and the stable release dosage per day **(F)** are shown for the administration of SM-345431 using this novel DDS. **(G)** Exposed intact spinal cord. **(H)** Transected spinal cord. **(I)** The novel DDS we employed. A silicone sheet containing SM-345431 was placed onto the transected site of the spinal cord. The system allowed for stable and continuous release of the semaphorin3A inhibitor throughout the experimental period.

The release of SM-345431 (0.1 mg/mg loading 10%) *in vivo* was calculated as 0.5-0.7 μg/day, and this dose was similar to the dose of the semaphorin3A inhibitor (SM-216289) [19] that we administered using osmotic mini pumps in our previous study [20]. Therefore, the newly developed DDS allowed stable and continuous release of the newly developed, potent semaphorin3A inhibitor SM-345431.

SM-345431 delivery via the novel DDS enhanced axonal regeneration

To examine the regeneration of axons after SM-345431 treatment and SM-345431 treatment combined with extensive treadmill training, we evaluated axons in the injured spinal cord with immunostaining using antibodies against GAP43 and serotonin (5-HT) (Figure 2), GAP43 is widely used as a marker for regenerated axons. In both treatment groups, a marked increase in the number of GAP43-positive axons was observed at the epicenter of the injury (Figure 2D-F) and in the surrounding area (Figure 2G-I). Compared with the control group, the number of GAP43 axons was significantly increased in both the SM-345431 treatment group and the combined treatment group, especially at 1 mm caudal to the injury epicenter (Figure 2J). No significant difference was observed between the 2 treatment groups. Thus, administration of the semaphorin3A inhibitor SM-345431 using this DDS enhanced axonal

Table 1 Pharmacological profile of SM-345431 (part 1)

Enzymes	IC50 (μm)
Semaphorin	0.1-0.2
Matrix Metalloproteinase-1 (MMP-1)	>10
Matrix Metalloproteinase-7 (MMP-7)	10
Matrix Metalloproteinase-2 (MMP-2)	>10
Matrix Metalloproteinase-3 (MMP-3)	>10
Matrix Metalloproteinase-9 (MMP-9)	>10
Phospholipase PLA2-1	>10
Phospholipase PLC	>10
Caspase 1	>10
Caspase 3	>10
Caspase 6	>10
Caspase 7	>10
Caspase 8	>10
Protein Tyrosine Phosphatase, CD45	>10
Protein Tyrosine Phosphatase, PTP1B	>10
Protein Tyrosine Phosphatase, PTP1C	>10
Protein Tyrosine Phosphatase, T-Cell	>10
Sphingomyelinase, Neutral (N-SMase)	>10
Chemokine CCR1	>10
Chemokine CCR2B	>10
Chemokine CCR4	>10
Chemokine CCR5	>10
Chemokine CXCR2 (IL-8B)	>10
Glucocorticoid	>10
Interleukin IL-1	>10
Interleukin IL-2	>10
Interleukin IL-6	>10
Tumor Necrosis Factor (TNF), Non-selective	>10
Adhesion, fibronectin-mediated	>10
Adhesion, ICAM-1-Mediated	>10
Adhesion, VCAM-1-Mediated	>10
Cell proliferation, B-Cell+LPS	>10
Cell proliferation, T-Cell+Con A	>10
Mediator release, IL-1beta	>10
Mediator release, IFN-gamma	>10
Mediator release, IL-10	>10
Mediator release, IL-2	>10
Mediator release, IL-4	>10
Mediator release, IL-5	>10
Mediator release, IL-6	>10
Mediator release, TNF-alfa, PBML	>10
Transcription response, NF-AT	>10
Transcription response, NF-kB	>10

Summary of the IC50 values for binding assays of various receptors and ion channels, and IC50 values for the inhibition of various enzymes. The IC50 value for semaphorin3A inhibition was extremely low compared to that of the other factors.

Table 2 Pharmacological profile of SM-345431 (part 2)

Kinases	IC50 (μm)
CaMKII	>10
CDK5/p35	>10
cSRC	>10
EGFR	0.90
EphA2	>10
EphA4	0.80
EphB2	0.68
EphB4	>10
Fes	>10
FGFR1	>10
FGFR2	>10
FGFR3	0.77
FGFR4	0.64
Flt1	>10
Flt3	>10
Fyn	>10
GSK3α	2.46
GSK3β	>10
IGF-1R	>10
JAK3	>10
KDR	>10
MAPK2	>10
MEK1	>10
MEK4	>10
MKK6	>10
PAK2	>10
PAK4	>10
PKA	>10
PKBα	>10
PKBβ	>10
PKCγ	>10
ROCK-I	>10
ROCK-II	>10
ROCK-II	>10
SAPK2a	>10
TrkA	>10
TrkB	>10
PI 3-Kγ	>10

Summary of the IC50 values revealed by inhibition tests for various kinases. The data in Tables 1 and 2 suggest that SM-345431 was highly selective for semaphorin3A inhibition.

regeneration. However, no additional axonal regeneration was observed when SM-345431 treatment was combined with treadmill training.

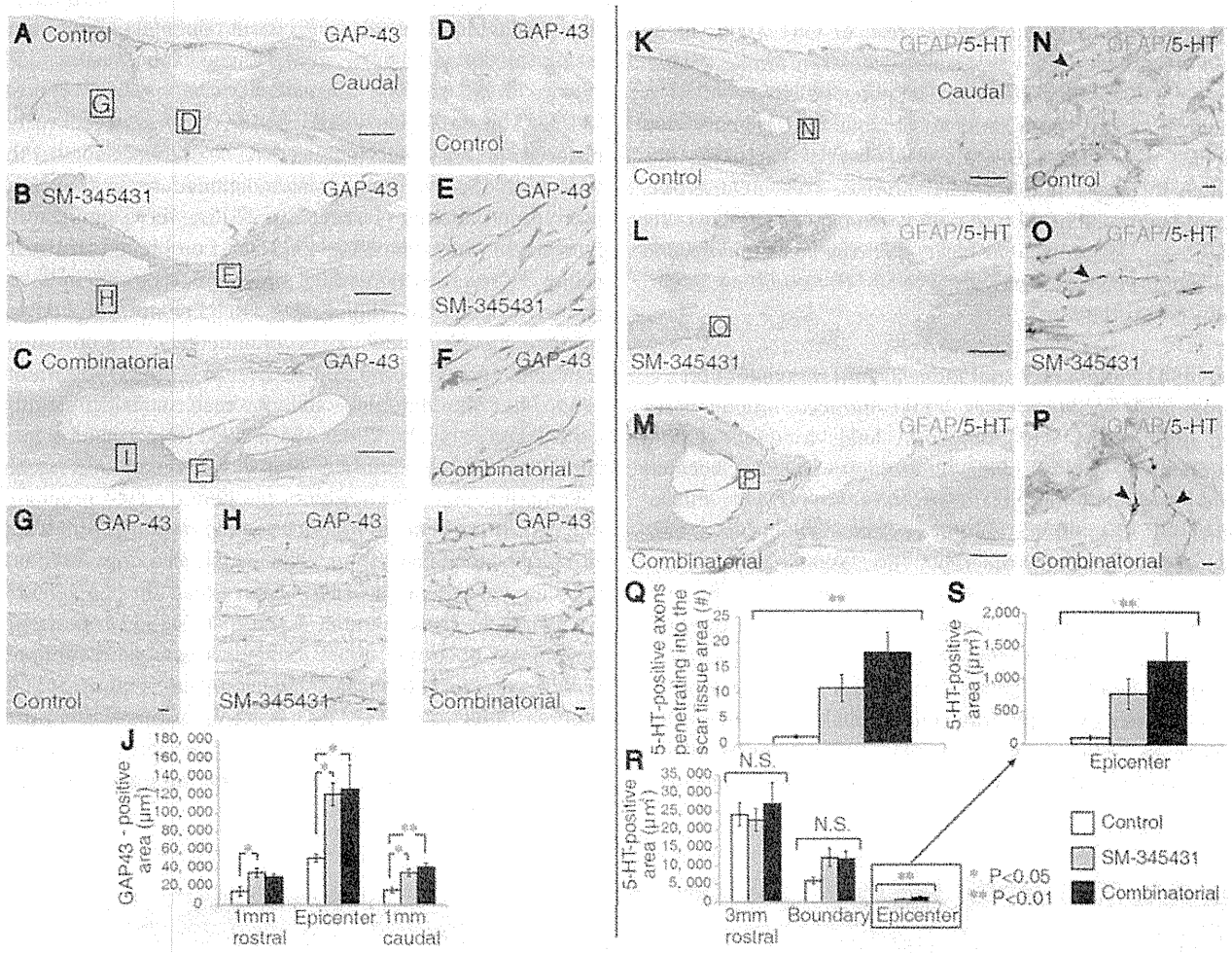

Figure 2 SM-345431 enhanced axonal regeneration *in vivo*, but combined treatment had only a limited effect on further axon regeneration. (A-I) Sagittal sections from SCT rats immunostained for GAP-43. Low-magnification images of the control **(A)**, SM-345431 **(B)** and combined treatment **(C)** groups. Scale bars = 500 μm. **(D-F)** Magnified images of the boxed areas shown in **A-C**. Scale bars = 10 μm. **(G-I)** Additional magnified images of the boxed areas shown in **A-C**. Scale bars = 10 μm. **(J)** Quantitative analysis of GAP-43-positive areas at 1 mm rostral to the lesion, 1 mm caudal to the lesion and at the epicenter of the lesion. Immunohistochemistry was performed using DAB with nickel enhancement. *P < 0.05, **P < 0.01. Statistical analyses were performed using one-way ANOVA and Bonferroni post hoc tests. Data are represented as the mean ± S.E.M. **(K-P)** Sagittal sections of SCT rats double-stained for 5-HT and GFAP. Scar tissue is outlined by GFAP staining, which also allowed for confirmation of total transection of the spinal cord in each animal. **(K-M)** Low-magnification images of the control **(K)**, SM-345431 **(L)** and combined treatment **(M)** groups. Scale bars = 500 μm. **(N-P)** Magnified images of the boxed areas shown in **K-M**. Scale bars = 10 μm. Arrowheads represent 5-HT-positive (serotonergic) axons. **(Q-S)** Quantitative analyses of 5-HT-positive axons that penetrated into the scar tissue. **(Q)** Quantitative analysis of the number of 5-HT-positive axons that penetrated into the lesion site. **(R,S)** Quantitative analysis of the 5-HT-positive area within the scar tissue area. Immunohistochemistry was performed by double-staining using DAB with or without nickel enhancement. The left side is rostral in all images. **P < 0.01. Statistical analyses were performed using a Kruskal-Wallis H test. Data represent the mean ± S.E.M.

The raphespinal tract axons, which can be detected by immunohistochemistry against serotonin (5-HT), contribute to functional locomotor control, and regeneration of these axons leads to substantial enhancement of motor function recovery [28]. Therefore, we also evaluated the regeneration of raphespinal tract axons using a GFAP antibody to delineate scar tissue at the injury site and a 5-HT antibody to visualize raphespinal axons. In control animals, 5-HT-positive axons were restricted to the area rostral to the transected site, and few 5HT-positive axons entered the GFAP-negative scar tissue area (Figure 2K,N). Interestingly, significantly more 5-HT-positive axons penetrated the GFAP-negative scar tissue area after SM-345431 treatment and combined treatment as compared to the control conditions (Figure 2K-S). Because we used a total transection model in this study, the 5-HT-positive axons that penetrated the GFAP-negative scar tissue in the treatment groups were regarded as regenerated axons (Figure 2L-P). Cortico-spinal tract (CST) axons are known to be incapable of regeneration after transection, even

following any of the previously reported treatments [7]. We next evaluated the regeneration of CST axons using the anterograde tracer biotinylated dextran amine (BDA). We first confirmed sufficient labeling efficiency of BDA tracing in each animal, and no obvious CST regeneration beyond the lesion epicenter was observed in either the control or the semaphorin3A inhibitor treatment group, which is consistent with our previous paper's findings [20] (Figure 3). Moreover, no clear CST regeneration beyond the lesion epicenter was observed in the combined treatment group (Figure 3).

SM-345431 enhanced angiogenesis and remyelination

Semaphorin3A suppresses VEGF-induced angiogenesis, and inhibition of semaphorin3A leads to enhancement of angiogenesis [29]. This phenomenon occurs because semaphorin3A and VEGF share the same receptor, neuropilin1 [30]. In addition, blood vessels are believed to play important roles in tissue repair and axonal regeneration after SCI [31-33]. Therefore, we analyzed the effects of SM-345431 treatment (using our DDS) on angiogenesis. For immunohistochemistry, we used the anti-RECA-1 antibody, which is known to enable visualization of blood vessels and migrating endothelial cells in rats [32] (Figure 4A). RECA-1-positive areas 3 mm caudal to the lesion epicenter were significantly increased after combined treatment (Figure 4C, $P < 0.05$). Based on their morphology, thick-walled blood vessels with lumen diameters larger than 20 μm are thought to be newly formed blood vessels [34] (Figure 4A,B, arrows). Consistent with previous reports [34,35], these thick-walled blood vessels were rarely observed in the intact spinal cord. In comparison to the control group, the total immunostained areas of vessels with lumen diameters larger than 20 μm were significantly increased in both the SM-345431 and combined treatment groups 3 mm rostral/caudal and 1 mm rostral/caudal to the lesion epicenter (Figure 4D). Furthermore, the effects of angiogenesis tended to be enhanced in the combined treatment group compared to the SM-345431 treatment group, but this difference did not reach statistical significance (Figure 4C,D). Thus, SM-345431 treatment significantly increased the number of newly formed blood vessels.

Semaphorin3A also inhibits oligodendrocyte precursor cell recruitment and influences remyelination [36]. Using immunohistochemistry and electron microscopy, we next characterized the axons at the lesion sites after SM-345431 treatment in greater detail. In the SM-345431 treatment group, we observed substantial numbers of myelinated GAP43-positive axons at the lesion site (Figure 4H-J), whereas myelinated GAP43-positive axons were rarely observed at the lesion site in the control SCT group (Figure 4E-G). Based on their morphologies, the thin

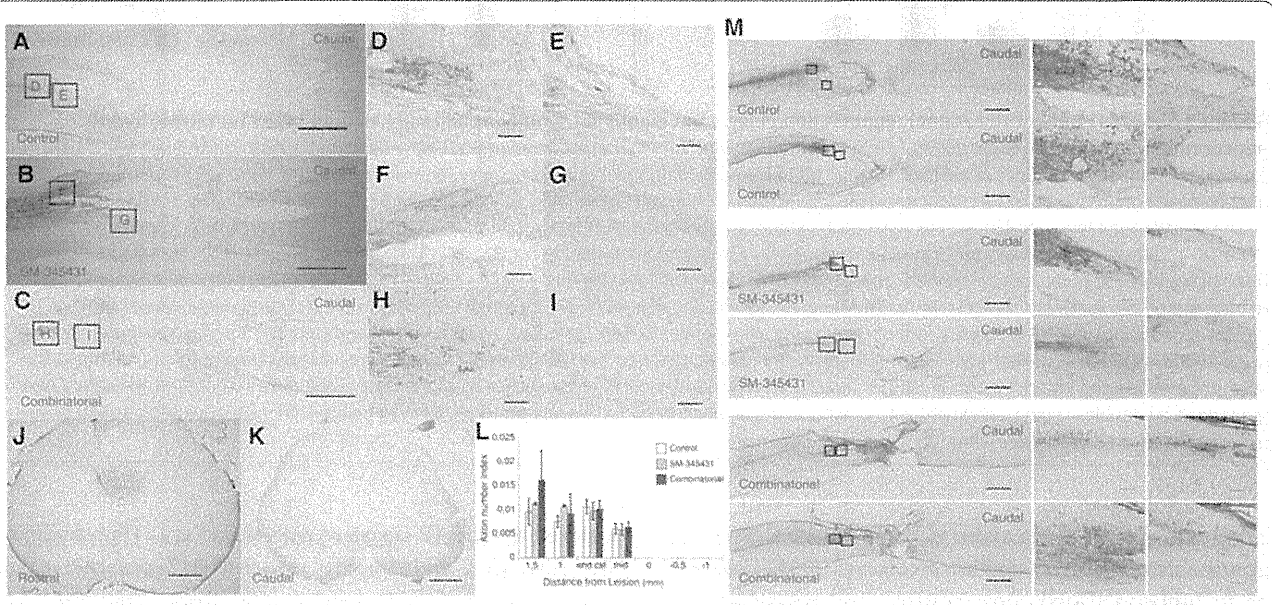

Figure 3 Histological analyses of the treatment effects on CST regeneration in the injured spinal cord using BDA staining. **J** shows a representative axial section of the spinal cord at the C4 level (rostral to the lesion site), and **K** shows a representative image of a section at the L4 level (caudal to the lesion site) (Scale bars = 500 μm). Based on these sections, we confirmed that the labeling efficiency of BDA tracing in each animal was sufficient. **A**, **B** and **C** show representative sagittal sections of the BDA staining in each group. **D**/**E** show magnified images of the boxed area in **A**. Similarly, **F**/**G** show magnifications of the areas in **B**, and the images in **H**/**I** are magnifications of the areas in **C**. Scale bars = 1,000 μm in **A**-**C** and 100 μm in **D**-**I**. No obvious CST regeneration beyond the lesion epicenter was observed in any of the groups examined (**L**). Statistical analyses were performed using one-way ANOVA and Bonferroni *post hoc* analyses. Data are presented as the mean ± S.E.M. The images in **M** are representative of other sagittal sections from each group. Scale bars = 1,000 μm in the images on left side of **M** and 100 μm in the magnified images of **M**.

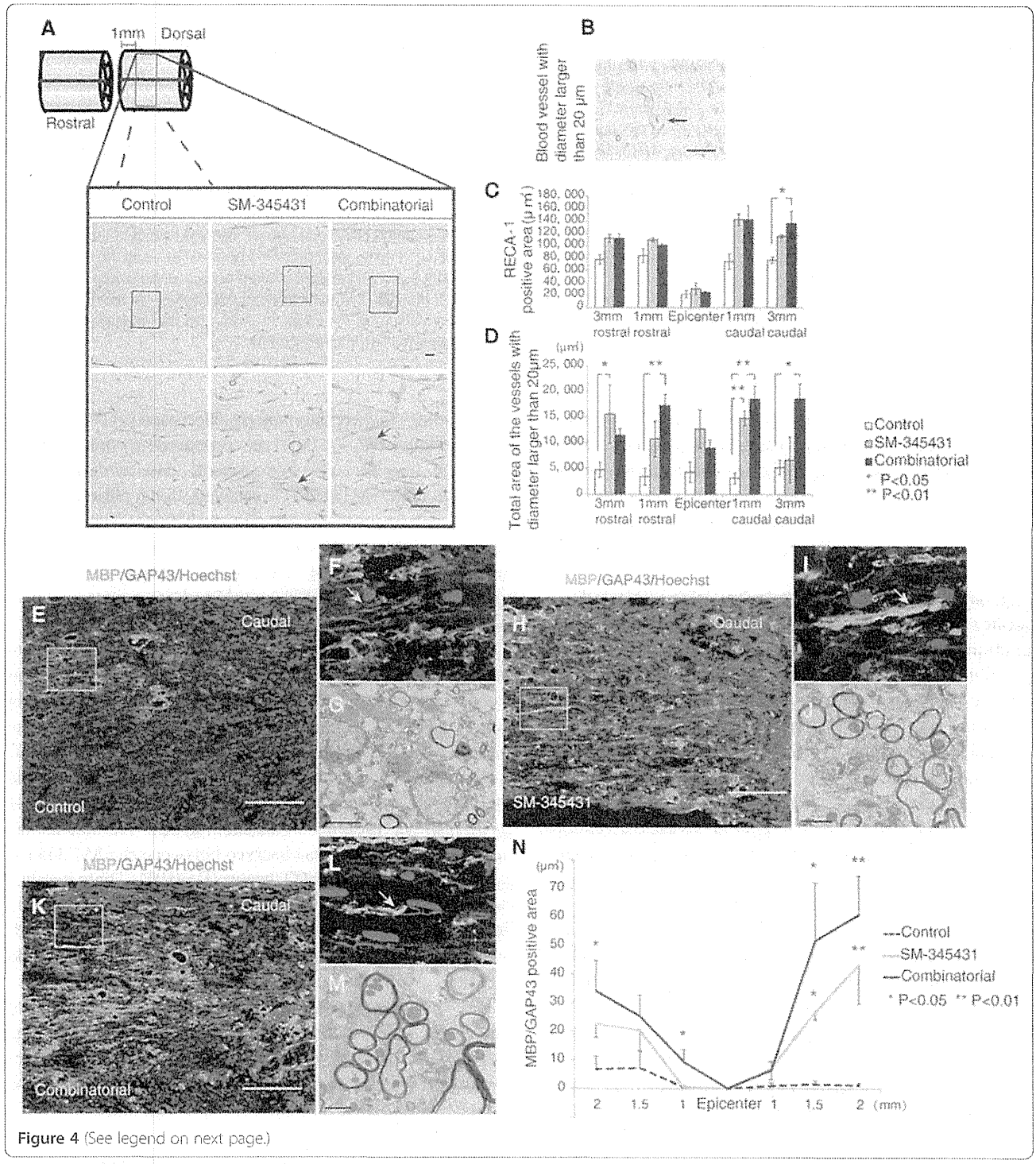

Figure 4 (See legend on next page.)

(See figure on previous page.)
Figure 4 Histological analyses of the treatment effects on microvasculature and remyelination in the spinal cord. (A) Visualization of blood vessels using an anti-RECA-1 antibody. Images in the upper row are low-magnification views of the gray matter areas of sagittal sections immunostained for RECA-1 at 1 mm caudal to the transected site. Scale bars = 50 μm. Images in the lower row are high-magnification views that correspond to the boxed areas in the upper row images. Scale bars = 50 μm. **(B)** Representative image of a blood vessel with a lumen with a diameter larger than 20 μm (arrow), which indicated newly formed blood vessels following injury. Scale bars = 50 μm. Arrows in **(A)** also represent blood vessels with lumen diameters larger than 20 μm. The left side is rostral **(A,B)**. **(C)** Quantitative analysis of RECA-1-positive areas in each group. **(D)** Quantitative analysis of the total areas of RECA-1-positive blood vessels with lumen diameters larger than 20 μm. *P < 0.05, **P < 0.01. Statistical analyses were based on one-way ANOVA and Bonferroni post hoc analyses. **(E-M)** Analyses of remyelination performed using immunohistochemistry against MBP or electron microscopy 12 weeks post-injury. **(E,F,H,I,K,L)** Reconstructed confocal images showing double staining (sagittal sections) for MBP (green) and GAP43 (red) in the control group **(E,F)**, SM-345431 treatment group **(H,I)** and combined group **(K, L)**. **F**, **I** and **L** show magnified images of the boxed areas in **E**, **H** and **K**, respectively. Scale bars = 100 μm. The arrow in **F** shows a non-myelinated (MBP-negative) GAP-43-positive axon, and the arrows in **I** and **L** show myelinated (MBP-positive) GAP-43-positive axons. The left side is rostral. **(G,J)** Electron microscopic images of transverse sections from the control group **(G)** and SM-345431 treatment group **(J)** at the lesion site. Scale bars = 2 μm. **(N)** Statistical analysis of the number of myelinated (MBP-positive) GAP-43-positive axons in each group, which were analyzed by immunohistochemistry. *P < 0.05, **P < 0.01. Statistical analyses were performed using one-way ANOVA and Bonferroni *post hoc* analyses. All the data are represented as the mean ± S.E.M.

myelin sheathes observed in the SM-345431 group were likely the result of remyelination (Figure 4H-J). While SM-345431 treatment significantly enhanced the remyelination of axons (Figure 4N), additional remyelination was not observed in the SM-345431 plus treadmill training combined group (Figure 4K-N).

Combining SM-345431 with treadmill training reinforced specific spinal locomotor circuitry and synaptic connectivity

Functional locomotor recovery in spinal cord models is critically dependent on supraspinal connections to CPGs [37]. To examine the combined effects of SM-345431 treatment and treadmill training on the reconstruction of spinal cord circuitry at the lumbar level, we performed immunostaining for c-Fos [38] and synapsin-1 [39,40]. c-Fos is widely used as a marker to measure the extent of the supraspinal drive of specific spinal locomotor circuitries because c-Fos expression in neurons normally increases when after the control of spinal locomotor circuitries' circuitry control is lost [41,42]. Consistent with previous studies, c-Fos expression in nuclei (c-Fos + nuclei) was observed in all rats in levels L1-L5 (Figure 5A-C) [43]. In addition, the number of c-Fos + nuclei tended to be lower at the L1-L5 levels in SM-345431-treated SCI rats than in control SCI rats, but this difference did not reach statistical significance (Figure 5B). Interestingly, the combined treatment group showed a statistically significant decrease in the number of c-Fos + nuclei compared to control SCT rats at the L4 and L5 levels (Figure 5B, $P < 0.01$). We also compared the rostral (L1 + L2) and caudal (L4 + L5) segments of the lumbar enlargement to examine the overall effects of combinatorial treatment (Figure 5C). Compared to the intact group (normal rats), control SCT rats showed a significant increase in c-Fos + nuclei counts in the caudal segments of the lumbar enlargement (L4-5), which is consistent with previous reports (Figure 5C, $P < 0.01$) [24]. On the other hand, after combined treatment, the caudal segments of the lumbar enlargement showed significantly decreased c-Fos + nuclei counts (Figure 5C, $P < 0.01$) as compared to control SCT rats. The number of c-Fos + nuclei also tended to be decreased after SM-345431 treatment alone, although this difference was not statistically significant (Figure 5C). Thus, specific spinal locomotor circuitries, especially in the caudal sections of the lumbar enlargement, were considerably reinforced by combined treatment and, to a lesser extent, by SM-345431 treatment alone.

Synapsin-1, a widely used presynaptic marker, has been used to examine activity-dependent synaptic plasticity and synaptic function [39,40]. In comparison to the control and SM-345431 groups, a statistically significant increase in synapsin-1 expression was observed at the lumbar enlargement level (Figure 5E-N) ($P < 0.01$ compared to the control SCT group; $P < 0.05$ compared to the SM-345431 group) in the combined treatment group. No statistically significant difference was observed between the SM-345431 group and the control SCT group ($P > 0.05$). These results indicated that, while SM-345431 treatment alone had a limited effect, SM-345431 treatment combined with treadmill training significantly reinforced synaptic plasticity and function at the lumbar enlargement level.

Taken together, these data suggest that reinforcement of specific spinal locomotor circuitries and motor learning occurred in the lumbosacral circuits of adult rats after combined treatment. These effects were also observed, to a lesser extent, after SM-345431 treatment alone.

SM-345431 promoted motor functional recovery and combined treatment enhanced this recovery

Next, we investigated the hindlimb motor functions of rats while they walked on a treadmill (induced by a robotic device) using kinematic analysis. In the control SCT rats, hindlimb motor functions showed almost no recovery throughout the period of our experiments (3 months). The SCT rats were unable to take any steps on a treadmill even 3 months post-injury, whereas the treated animals

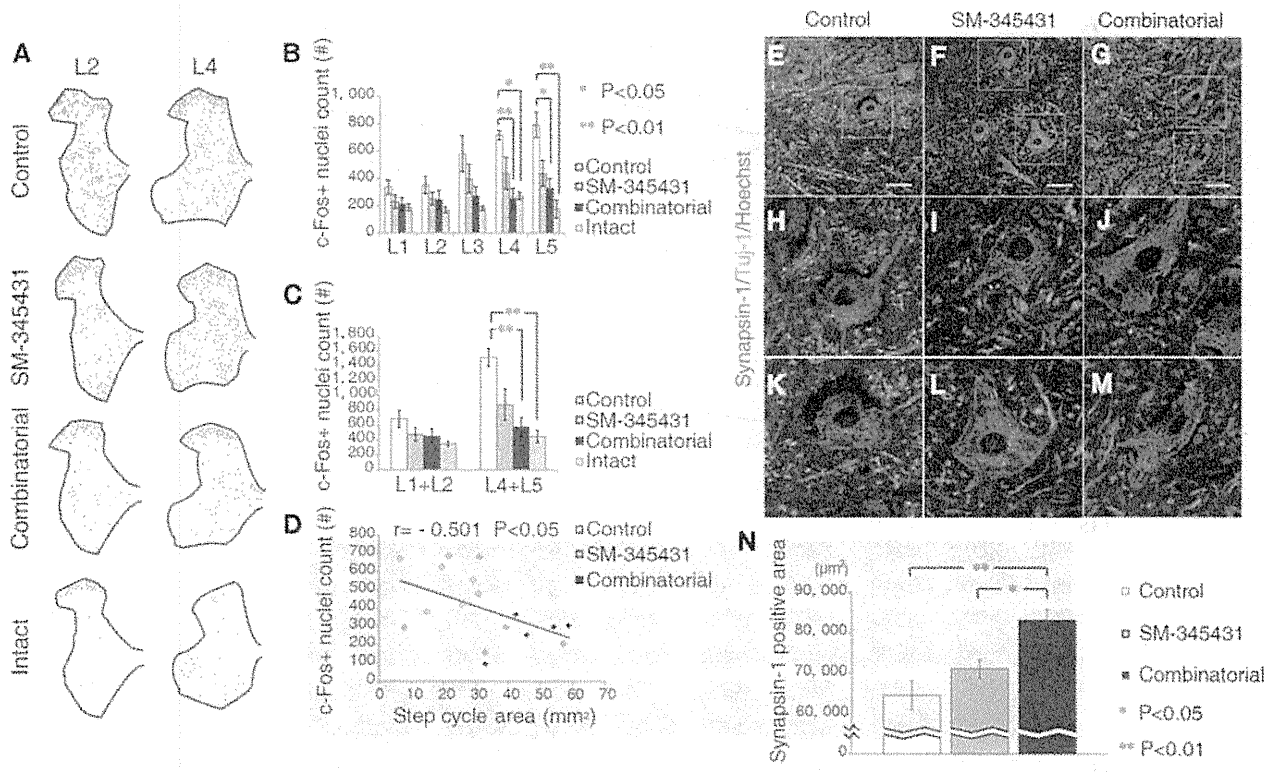

Figure 5 Immunohistochemical analyses of the effects of treatment on functional remodeling of spinal circuits and synaptic connectivity at the lumbar enlargement. **(A)** Representative Camera Lucida drawings of c-Fos + nuclei in transverse sections at the L2 and L4 levels from control rats, SM-345431 treatment rats, combined treatment rats and intact rats. **(B)** Average total numbers of c-Fos + nuclei at each level of the lumbar spinal segment. **(C)** Average total number of c-Fos + nuclei in rostral (L1 + L2) and caudal (L4 + L5) lumbar enlargement segments. **(D)** Correlation analysis between the total number of c-Fos + nuclei in all segments of the lumbar enlargement and step ability on the treadmill. SM-345431 treatment produced a trend toward decreases in the average number of c-Fos + nuclei, although this trend was not statistically significant compared to the control and SM-345431 treatment groups. However, the combined treatment produced a statistically significant decrease in the number of c-Fos + nuclei, suggesting that specific spinal locomotor circuitry was reinforced by combining SM-345431 treatment with extensive treadmill training. *P < 0.05, **P < 0.01. Statistical analyses were performed using one-way ANOVA and Bonferroni post hoc analyses. Data are presented as the mean ± S.E.M. **(E-M)** Representative reconstructed confocal images of double staining (transverse section) for synapsin-1 and Tuj-1 in the ventricolumnar area of the spinal cord (**E-G**: low-magnification images, **H-M**: high-magnification images). **H-J** and **K-M** show the upper and lower boxed areas in **E-G**, respectively. Scale bars = 50 μm. **(N)** Quantitative analysis of synapsin-1 expression in the ventricolumnar motor neuron area 3 months after SCT. *P < 0.05, **P < 0.01. Statistical analyses were performed using one-way ANOVA and Bonferroni *post hoc* analyses. Data are presented as the mean ± S.E.M.

showed some degree of motor function recovery. We performed Bonferroni *post hoc* analyses to examine the differences in step length and step height between the groups (Figure 6A) and found that motor function was significantly better in SM-345431 rats than in control SCT rats (Figure 6B-C). Furthermore, SM-345431 treatment with treadmill training further improved motor performance as compared to no treatment (Figure 6B,C,D,E) or SM-345431 treatment alone (Figure 6D,E). To evaluate motor functions in greater detail, we examined the "step cycle area", which was calculated by multiplying the average step length and average step height as previously described [44] (Figure 6F). This parameter includes elements of both the horizontal and vertical step planes and can thus be regarded as a 2-dimensional evaluation of each step taken. We again performed Bonferroni *post hoc* analyses to statistically compare the differences between the groups. In the SM-345431-treated rats, a statistically significant enhancement of the step cycle area was observed in comparison to the control SCT rats ($P < 0.05$ at 3 months). Furthermore, the combined treatment resulted in an even greater improvement in step cycle area when compared to control SCT rats ($P < 0.05$ at the first month, $P < 0.01$ at the second month, $P < 0.01$ at the third month). As previously described [20], the control SCT rats could not take any steps on the treadmill even at 3 months post-injury (Figure 6G,H and Additional file 1). Without extensive treadmill training, the effects of SM-345431 treatment were moderate and did not result in plantar step walking, even with the BSS (Figure 6G,H and Additional file 1). However, when combined with extensive treadmill training, SM-345431 treatment led

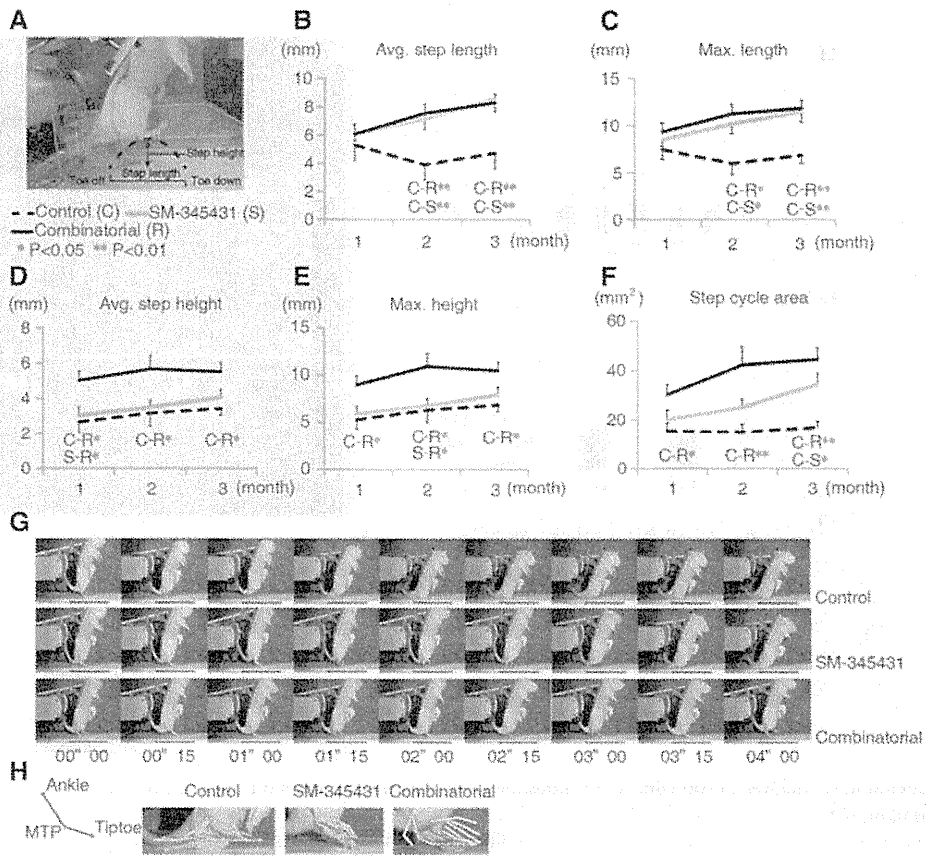

Figure 6 Detailed kinematic analysis of hindlimb motor performance on the treadmill. (A) Representative image of the analysis and a schematic diagram of the step parameters. Collected kinematic data from each group showing the average step lengths **(B)**, maximum step lengths **(C)**, average step heights **(D)**, maximum step heights **(E)** and step cycle areas **(F)**. All of these data were recorded and analyzed using a robotic device (Rodent Robot 3000; Robomedica Inc.). Each kinematic analysis was performed at 70% BWS and a speed of 1 cm/s over 1 min. C represents the control group, S represents the SM-345431 group, and R represents the combined treatment group. *P < 0.05, **P < 0.01. C-S* indicates that a statistically significant difference was observed between the control and SM-345431 groups at P < 0.05. Statistical analyses were performed using one-way ANOVA with Bonferroni *post hoc* analyses. Data are presented as the means ± S.E.M. **(G)** Representative sequential pictures of steps taken during the first 4 s of the analysis (BWS: 70%, speed: 3 cm/s). **(H)** Kinematic characteristics of the first step taken in each group. SM-345431 treatment enhanced motor function recovery on the treadmill, especially in terms of the step length parameters. Combined treatment further enhanced the motor function recovery, especially in terms of the step height and step cycle area parameters.

to considerably enhanced motor function recovery; all rats exposed to the combined treatment achieved continuous plantar step walking on a treadmill with the BSS for at least 30 min (Figure 6G,H and Additional file 1).

Specifically, SM-345431 treatment improved locomotor function on a treadmill after SCT particularly in terms of the step length parameters (Figure 6B,C: average and maximum step lengths). Regarding the step height parameter, the effect of SM-345431 treatment was moderate and statistically insignificant (Figure 6D,E). However, when SM-345431 treatment was combined with extensive treadmill training, greater enhancement was observed, and this enhancement extended to the step height parameter (Figure 6D,E; average and maximum step heights). Furthermore, the incremental effects of the treatments over time on motor function performance, specifically on step height and step cycle area, did not reach a plateau by the end of the experimental period (3 months post-injury). At this time, the incremental effects tended to be more robust in the SM-345431 treatment group than in the combined treatment group (Figure 6F: step cycle area). Interestingly, we also discovered a statistically significant correlation between the number of c-Fos + nuclei and motor function (step cycle area) within each group; the c-Fos + nuclei counts were inversely correlated with the extent of functional motor recovery (Figure 5D; r = -0.501, P < 0.05).

We next examined the extent to which the regenerated axons at the lesion sites contributed to motor function recovery in each group. We performed re-transection of the initial lesion site 12 weeks after the initial injury, and we also performed the kinematic analysis before and after the re-transectioning procedure. None of the step parameters changed significantly in the control group, whereas the

step cycle area tended to be attenuated in the SM-345431 group after re-transection (Figure 7). Interestingly, greater attenuations of step ability were observed in all analyzed parameters in the combined treatment group after re-transection, and some of these parameters (step height) were statistically significant (Figure 7, average step height: $P < 0.01$; maximum step height: $P < 0.05$). Thus, the regenerated axons at the lesion site contributed, at least partially, to the enhancement of motor function recovery.

Discussion

With clinical applications in mind, we first sought to find an appropriate and efficient way to deliver our semaphorin3A inhibitor to transected spinal cords to reestablish useful motor function after SCI. For this purpose, we developed a novel DDS and tested its therapeutic potential *in vivo*. Furthermore, we tested whether specific rehabilitation had the capability to reinforce motor function in the SCT model after treatment with the semaphorin3A inhibitor. Our results can be briefly summarized as follows. First, our newly developed DDS utilizing silicone sheets provided continuous and stable drug delivery and therefore demonstrated potential clinical application. Second, motor function recovery was considerably enhanced by combining SM-345431, the novel semaphorin3A inhibitor, with treadmill training, and this combined treatment enabled paralyzed rats to perform continuous plantar step walking on a treadmill with a BSS.

Osmotic mini pumps have been widely used for drug delivery in animal models of SCI [20,45]. While these pumps are excellent for controlling the drug release dosage and the accurate positioning of drug delivery, this method is too invasive for use in most patients. Therefore, we developed a new silicone matrix preparation as a novel DDS and showed that this novel DDS provided stable and continuous release of SM-345431 throughout the experimental period. In addition, because SM-345431 shows a better stability in a silicone sheet than SM-216289 and approximately the same semaphorin3A inhibitory activity as SM-216289, we used SM-345431 instead of SM-216289 in the present study. As a result, significantly enhanced axonal regeneration and motor function recovery were observed after SM-345431 treatment, which is consistent with our previous study using SM-216289 and osmotic mini pumps [20]. Therefore, this novel DDS demonstrated strong potential for future clinical use.

In this study, we examined the effects of a new semaphorin3A inhibitor, SM-345431, on axonal regeneration and motor function recovery after SCT. Our data indicated that SM-345431 administration using the novel DDS was effective in promoting axonal regeneration and motor function recovery *in vivo*. However, consistent with the results of our previous study using SM-216289, these effects were moderate [20]. More importantly, we found that motor function recovery was significantly enhanced by combining SM-345431 with extensive treadmill training (Figure 6). This combined strategy enabled paralyzed rats to perform continuous plantar step walking on a treadmill with a BSS. Previous work has also demonstrated that intact or injured axons in descending tracts and propriospinal circuits can undergo spontaneous anatomical and physiological remodeling after SCI [46,47] to allow the relay of information through endogenous spinal circuits. Subsequently, the novel propriospinal relay connections bypass the injury epicenter to induce supraspinal control and some degree of motor function recovery. This phenomenon has also been observed following the irreversible interruption of long descending tracts in mice [48]. Because SM-345431 treatment without extensive treadmill training had limited effects on anatomical reconstruction in the lumbar enlargement

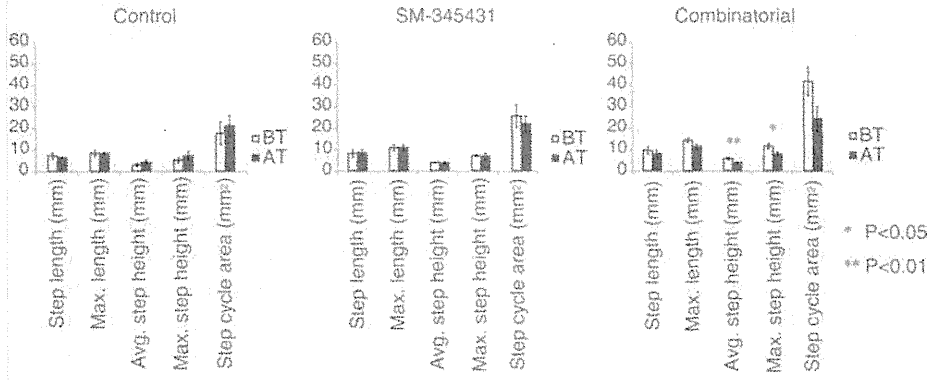

Figure 7 Detailed kinematic analyses of hindlimb motor performance on a treadmill before and after re-transection. Detailed kinematic analyses of hindlimb motor performance on a treadmill before and after re-transection were performed and analyzed using a robotic device (Rodent Robot 3000; Robomedica Inc.). BT represents before re-transection; AT represents after re-transection. Although none of the step parameters in the control group showed significant changes, the step cycle area parameters were attenuated in the SM-345431 group after re-transection. Further attenuation of the step ability parameters was observed in the combined treatment group after re-transection. *$P < 0.05$ **$P < 0.01$. Statistical analyses were performed using *t*-test analyses. Data are presented as the mean ± S.E.M.

(Figure 5), we speculate that the enhanced motor function recovery observed after SM-345431 treatment resulted mainly from axon regeneration and limited anatomical reconstruction. Enhanced axonal regeneration possibly led to anatomical and physiological remodeling at the lesion site and improved motor function recovery, which is consistent with our previous findings using SM-216289 administered via osmotic mini pumps [20].

Interestingly, while axonal regeneration was not further enhanced by combining SM-345431 treatment with extensive treadmill training (Figure 2), motor function recovery was significantly enhanced (Figure 6). Previous work demonstrated that limited spontaneous axonal regeneration occurs after SCI and that only some of the new axons are useful for motor function recovery [49]. Thus, axonal regeneration alone may not result in sufficient motor function recovery unless these regenerated axons are appropriately connected. We therefore hypothesized that the regenerated axons induced by semaphorin3A inhibitor treatment may exhibit substantially improved rewiring, in terms of the formation of appropriate connections, following extensive treadmill training. Indeed, motor function recovery was enhanced significantly by combined treatment, as paralyzed rats that received combined treatment were able to perform continuous plantar step walking on a treadmill with a BSS (Figure 6). Re-transectioning experiments further suggested that the regenerated axons at the lesion site and their rewiring contributed to the enhancement in motor function recovery observed in the treatment groups (Figure 7). We also observed that some regenerated axons, such as 5-HT-positive raphespinal tract axons, penetrated into the epicenter of the lesion (Figure 2), and these regenerated axons may have contributed to the reorganization of spinal circuitry at the lesion site and enhanced motor function recovery in the treatment groups [20]. Interestingly, we observed greater attenuation of motor function after re-transection in the combined treatment group (Figure 7). Taken together, these data indicate that the regenerated axons achieved substantial rewiring to the appropriate targets at the lesion site, which was associated with the rehabilitation performed in the combined treatment group [21].

Moreover, the enhanced motor function recovery was only partially attenuated after re-transection in the treatment groups. The results of these re-transection experiments in the treatment groups, especially in the combined treatment group, suggested that other factors, such as reorganization of the lumbar spinal circuitry, also contributed to the enhancement of motor function recovery. We also performed re-transection experiments in animals that only received extensive treadmill training (without SM-345431 treatment), and in these animals, only minimum attenuation of motor performance after re-transection was observed (data not shown). This finding further supports the mechanism proposed above. Taken together, it is possible that specific rehabilitation enhances not only the rewiring of the regenerated axons but also the reorganization of the lumbar spinal circuitry [43]. Furthermore, in the combined treatment group, it is possible that the effect of specific rehabilitation on the reorganization of the lumbar spinal circuitry was the main contributor to the enhancement of motor function recovery in the early stage, while the effect on rewiring of the regenerated axons was the main contributor to the enhancement of motor function recovery during the later stage.

The results of c-Fos immunohistochemistry (Figure 5) showed that extensive treadmill training induced plastic changes at a level caudal to the injured site. Interestingly, step ability on the treadmill was significantly correlated with decreases in the numbers of c-Fos-positive nuclei at a level caudal to the lumbar enlargement (Figure 5D). Therefore, enhanced motor function recovery could be partially the result of anatomical reconstruction of the lumbar spinal cord, which is thought to be the location of CPGs [50]. It is now widely accepted that supraspinal drive of CPGs is required for locomotor function [51] and that the intrinsic plasticity of CPGs allows some spontaneous motor function recovery even in the absence of significant axonal regeneration [24,52]. Therefore, it is possible that axon regeneration moderately enhanced motor function recovery in the SM-345431 treatment group, while rewiring of the regenerated axons and CPG activation was achieved by combining the SM-345431 treatment with treadmill training.

Which segment of the lumbar enlargement is most important for improved walking ability on a treadmill? Reportedly, rhythmic bursts are related to flexor activity at the L2 level and to extensor activity at the L5 level [50]. Treadmill training induces plastic changes in the transmission of group I pathways to extensors that consequently support the recovery of weight-supported motion while standing [53]. The present study showed that combined treatment significantly altered c-Fos expression at the L4 and L5 levels (Figure 5B-C) and improved step height (Figure 6D-E) and continuous plantar step walking on the treadmill with a BSS (Figure 6G and Additional file 1). However, while SM-345431 alone improved step ability, this improvement did not lead to continuous plantar step walking (Figure 6). Therefore, axon regeneration alone might have only limited effects on the spinal cord extensor pool, which could explain the limited motor function recovery of SCT rats after SM-345431 treatment alone. However, the combined treatment may have reestablished the function of the extensor pool by rewiring the regenerated axons and remodeling spinal circuits. As a result, important motor functions, such as continuous plantar step walking (on a treadmill with a BSS), may have been reestablished in SCT adult rats in the combined

treatment group. Thus, combining SM-345431 treatment with specific rehabilitation is a reasonable and promising approach to the treatment of SCI.

Other possible mechanisms underlying motor function recovery could include remyelination and angiogenesis. We noticed that, with increases in afferent sensory input, the step lengths of the SM-345431 groups while walking on the treadmill exhibited a linear and gradual improvement throughout the experimental period. The animals treated with SM-345431 showed enhanced remyelination at the lesion site (Figure 4E-J), which could be relevant to a recent study reporting the effects of semaphorin3A on myelination [36]. In general, myelination significantly increases conduction velocity (sometimes up to 100-fold [54]), which results in increased motor function. Thus, remyelination after SM-345431 treatment may have also partially contributed to the enhancement of motor function recovery on the treadmill. Angiogenesis also plays an important role in reducing secondary damage and enhancing tissue repair after SCI, and the extent of angiogenesis correlates with the extent of axon regeneration after SCI [33]. Angiogenesis was significantly enhanced after SM-345431 treatment alone, although combined treatment did not further enhanced this effect statistically (Figure 4A-D). Therefore, angiogenesis may also have contributed to motor function recovery. Interestingly, at the end of the experimental period (3 months post-injury), the incremental effects of the treatment on motor performance, specifically in terms of step height and step cycle area, tended to be more robust in the SM-345431 treatment group than in the combined treatment group (Figure 6D-F). These data indicate that combined treatment may also have expedited motor function recovery and decreased the overall time needed for recovery.

Conclusions

Collectively, our data demonstrate that the administration of SM-345431 via a novel DDS utilizing silicone sheets significantly enhanced axonal regeneration, remyelination and angiogenesis, thereby promoting motor function recovery after SCT in adult rats. Additionally, combining SM-345431 with extensive treadmill training resulted in improved motor function recovery that included continuous plantar step walking on a treadmill with a BSS. This comprehensive effect of combined treatment presumably resulted from the reinforcement of spinal networks in the caudal spinal stump and the rewiring/refinement of regenerated axons. Thus, combining semaphorin3A inhibitor treatment with extensive treadmill training has great potential as a new treatment for SCI. In addition, this study highlights the importance of combining treatments that promote axon regeneration with specific and appropriate rehabilitations that promote rewiring for the effective treatment of SCI.

Methods

Overall experimental outline

Rats were randomly divided into the following three experimental groups: 1) untrained + placebo, 2) untrained + SM-345431 and 3) trained + SM-345431. SCT was performed, and SM-345431 or placebo was administered at the lesion site via the newly developed DDS, which is described in detail below. Starting 1 week post-injury, treadmill training commenced with a BSS. Kinematic tests were performed monthly for 3 months after SCT using a rodent robotic device (Rodent robot 3000, Robomedica Inc.) that primarily assessed the performance of plantar stepping on a treadmill. Treadmill training was continued throughout the experimental period.

Animals and surgical procedures

A total of 53 adult female Sprague-Dawley rats (200-250 g, 10-12 weeks old) were used in this study (3 rats died during the experimental period and were excluded from the statistical analysis). All procedures were approved by the experimental animal care committee of Keio University, School of Medicine and Murayama Medical Center (approval #12-8). All rats were anesthetized with an intraperitoneal injection of ketamine (100 mg/kg)/xylazine (10 mg/kg). The spinal cord at the level of the T10 lamina was exposed by T10 laminectomy, and the dorsal dura mater was opened. The exposed spinal cord was cut along the inner edge of the vertebra with a sharp micro-scissor. Two more cuts were made at the gap of the transected spinal cord by a scalpel to ensure total transection. SM-345431 or placebo was administered to the transected site via the newly developed DDS as described in detail below (Figure 1G-I). After these procedures, the back muscles and skin were closed. Rats were kept warm in an incubator (37°C) after surgery. To prevent dehydration in the rats, 10 ml of saline was subcutaneously injected daily until day 7. Ampicillin (0.4 g/kg) was also injected intramuscularly daily to prevent infection until day 7. The bladder was evacuated manually until autonomous emptying of the bladder was achieved. The re-transection procedure was performed at the same level as the primary SCT (15 rats total; 5 rats from each group). Kinematic data were recorded using similar procedures prior to re-transection surgery (on the same day) and on the day following re-transection surgery. For CST tracing, 10% BDA was injected as follows. Nine weeks after SM-345431 or placebo administration, BDA (10000 MW, Molecular Probes) was injected into six different sites of the sensorimotor cortices of the rats under general anesthesia (site 1: 2.0 mm lateral, 0 mm to bregma; site 2: 2.0 mm lateral, 2 mm posterior to bregma; site 3: 2.0 mm lateral, 4 mm posterior to bregma; site 4: 4 mm lateral, 0 mm to bregma; site 5: 4 mm lateral, 2 mm posterior to bregma and site 6: 4 mm lateral, 4 mm posterior to bregma). For

each site, injections were performed at two different depths (1.2 mm and 1.6 mm), and 3 μl of 10% BDA was injected at a rate of 0.15 μl/min using a micro-injector. Three weeks after the BDA injection, rats were sacrificed and used for immunohistochemistry.

Growth cone collapse assay and collagen co-culture assay

The growth cone collapse assay and collagen co-culture experiments were performed as previously described [20]. To examine the effects of SM-345431-silicone, small pieces (2 × 1 × 0.3 mm; approximately 1 mg containing 1 μg of SM-345431) of the SM-345431-silicone or control-silicone were placed in a collagen gel adjacent to E8 chick DRGs and COS7 cell aggregates, as shown in Figure 1C.

Drug delivery system

A novel matrix silicone preparation was developed to allow continuous drug delivery at the site of injury. The amount of drug released from this matrix silicone preparation *in vitro* was measured as described in Figure 1. Matrix silicone sheets (0.3 mm thick) containing SM-345431 were trimmed into 3-mm-square pieces to fit into the opened dura. After SCT, one piece of silicone sheet was placed on the transected spinal cord gap so that it could act on the spinal cord directly. Silicone sheets of the same size that did not contain SM-345431were used for the control group.

Training protocol

A robotic device (rodent robot 3000, Robomedica Inc.) [55] was used to train the SCT rats. Briefly, the device consisted of a computer-controlled BSS, two lightweight robotic arms and a treadmill with variable motorized speeds. The ankles of the hindlimbs of rats were held with a pair of releasable rope cuffs, which were then secured to robotic arms to track ankle trajectory in the horizontal and vertical directions. A computer-controlled body support arm was used to control the load that was applied to the hindlimbs and to maintain body equilibrium. Rats were secured in a cloth vest and attached to the body support arm with a hook-and-loop fabric. Hard rope cuffs were attached to the hindlimbs of rats with the robotic arm during training.

In our pilot study, we found that it was possible to train spinal cord-transected rats soon after SCT via voluntary walking evoked by sensory input. Additionally, improvements in motor performance were more obvious when the treadmill training was initiated at earlier time points after SCT. Therefore, training was initiated as early as 1 week after SCT. The fixed parameters were set at 50% body weight support (BWS), 20 min/day and 5 days/week. The animals were adapted to the training via increasing velocity; a velocity of 1 cm/s was used in the first week, and then the velocity was increased by 2 cm/s every 2 weeks for the first 2 months after injury (i.e., 1 cm/s to 3 cm/s to 5 cm/s). In the first week of training, rats frequently did not adapt to the acceleration of the treadmill, and this resulted in dragging of the hindlimbs. Once the rats dragged their hindlimbs and stopped walking on the treadmill, a trainer brought their bodies back to the original walking position. The step ability of SCT rats on the treadmill improved gradually over the course of the first 2 months following injury. However, this improvement was attenuated at time points later than 2 months after injury. Hence, at the time points later than 2 months after injury, the velocities of the treadmill were adjusted to 5 to 9 cm/s according to the improvement observed in the hindlimb motion of the rats.

Detailed motor function analysis using kinematics

To evaluate the locomotor capability of SCT rats in detail, the aforementioned robotic device was employed. Each robotic arm tracked the two-dimensional movement of the ankle, and the trajectory of the ankle movement was then recorded on a computer for kinematic analyses. Not all the rats were able to walk by themselves on the treadmill by the last time point of the experiment. Therefore, when performing the tests, the degree of BWS and treadmill speed were titrated to obtain the maximum walking performance on the treadmill. As a result of this titration, the behavioral tests were performed at 70% BWS and a treadmill velocity of 1 cm/s each month after SCT. The duration of testing was 1 min per rat to minimize training effects during testing. The methods of previous reports [44,56] were followed with slight adaptations. Briefly, the ankle trajectory in each plane was recorded by the robotic arm and a computer. Then, the toe off (TO) and paw contact (PC) events in each step cycle were identified using Rodent Robot 3000 software. All kinematic characteristics were obtained when TO and PC were identified; as a result, parameters such as the duration phase, the swing phase of the step cycle and the length and height of the step were calculated. The number of animals used in these behavioral tests was 32 (control: n = 9, SM-345431: n = 12, combined: n = 11).

Immunohistochemistry

Twelve weeks after SCT, rats were deeply anaesthetized by an intraperitoneal injection of 14% chloral hydrate and then perfused intracardially with 4% paraformaldehyde (PFA) in 0.1 M phosphate-buffered saline (PBS). The spinal cord tissues were dissected and post-fixed in 4% PFA (24 h) and placed in 10% sucrose in 0.1 M PBS (24 h) followed by 30% sucrose in 0.1 M PBS (24 h). All the rats other than 3 rats died during the experimental period were used for the histological analysis. Segments of spinal cords were embedded in Optimal Cutting Temperature compound (Tissue Tek) and stored at -80°C. Frozen spinal

cord tissues were cut with a cryostat into 20-μm-thick sections. For diaminobenzidine (DAB) staining, sections were washed with 0.1 M PBS and then presoaked for 30 min in 0.03% H_2O_2 with methanol. After an additional presoak in TNB (0.10 M Tris-HCl, 0.15 M NaCl, 0.5% BMP) for 60 min, sections were incubated at 4°C with rabbit anti-GAP43 (1:300; Millipore), mouse anti-rat RECA-1 (1:500; Serotec) or rabbit polyclonal anti-synapsin-1 (1:300; Chemicon) for 24 h. Subsequently, the sections were washed in 0.1 M PBS and incubated with biotinylated secondary antibodies (1:1,000; Jackson Immunoresearch) for 1 h. Next, the sections were washed and then incubated with an avidin-biotin complex (ABC) (Vectastain Elite ABC Kit, Vector Laboratories) in TNB (1:100) and visualized using DAB (Sigma). Sections were rinsed in PBS, dehydrated using ethanol and xylene and cover-slipped with permount. To identify 5-HT-positive axons that penetrated into the scar tissue area after the treatment, we used a previously described double-staining method [28]. 5-HT was visualized using goat anti-serotonin (5-HT) antibody (1:500; ImmunoStar) and DAB with nickel-glucose oxidase, which produced a black stain. Sections were washed and then incubated with rabbit monoclonal anti-glial fibrillary acidic protein (GFAP; 1:1,000; BD Bioscience Pharmingen) and visualized with DAB, which produced a brown stain. Following these procedures, we identified the range of the scars and quantified the number of 5-HT-positive axons that penetrated into the scar tissue area. To evaluate the status of axonal myelination, immunofluorescent double staining was performed using rabbit anti-GAP43 (1:1,000; Millipore) and rat monoclonal anti-MBP (1:50; Abcam) antibodies. Immunohistochemical analysis for c-Fos in spinal neurons was performed using procedures similar to those previously described [24,41,43]. Briefly, rats were trained using the aforementioned training method of continuous hindlimb bipedal stepping. After 45 min of continuous hindlimb bipedal stepping at 3 cm/s with 50% BWS with a hard nylon rope attachment, rats were allowed a 60-min rest. Subsequently, the rats were anesthetized and perfused intracardially with 4% PFA in PBS. After perfusion, the spinal cords were dissected, post-fixed for 24 h at 4°C and cryoprotected in 30% sucrose in PBS for 3 days. The L1-L5 segments were mounted and frozen, and 20-μm-thick axial sections were cut using a cryostat. All sections were pretreated with 0.03% H_2O_2 and methanol for 30 min and then incubated with rabbit polyclonal anti-c-Fos antibody (1:200; Santa Cruz Biotechnology) for 24 h (at 4°C). Subsequently, the sections were washed in 0.1 M PBS and incubated in biotinylated secondary antibody (1:1,000; goat antibody against rabbit; Jackson ImmunoResearch) for 1 h. The remaining procedures were identical to those performed for DAB staining, as described above. All images were obtained using either an Axioskop 2 Plus microscope (Zeiss) for DAB staining or a LSM510 confocal microscope (Zeiss) for immunofluorescent staining.

Electron microscopic analysis

For electron microscopic analysis, rats from the 3 groups were sampled 72 days after injury. Rats were perfused with 4% PFA in PBS, and the spinal cords were dissected and post-fixed with 2.5% glutaraldehyde overnight at 4°C. After 90 min of fixation with 0.5% osmium tetroxide, the spinal cords were dehydrated with ethanol, acetone and QY1 and then embedded. Ultrathin sections at the epicenter of the lesion sites were prepared at a thickness of 80 nm and stained with uranyl acetate and lead citrate for 15 and 12 min, respectively. The sections were observed with a transmission electron microscope (JEOL model 1230), and images were acquired using Digital Micrograph 3.3 (Gatan Inc.).

Quantitative immunohistochemistry analyses

Immunohistochemical image analyses were performed for all sections of each animal using microscopy, and quantitative analyses were performed by an examiner who was blind to the identities of the animals. Each value is presented as the average value per section (unless otherwise indicated). The number of animals used for quantitative analysis of each staining set ranged from 15 to 21 (5 to 7 animals per group). To quantify the area of GAP-43-positive axons, 5-HT-positive axons and RECA-1-positive vessels, sagittal sections of the spinal cord at the injury site (approximately 1.2 cm in length) were scanned with a CCD camera (DXC-390; Sony). Pictures of the sagittal sections at 1 mm to 3 mm rostral and 1 mm to 3 mm caudal from the injury epicenter were captured for quantitative analyses. The images were analyzed with a Micro Computer Imaging Device (MCID; Imaging Research Inc.). Threshold values were maintained at constant levels for all analyses. 5-HT axons that penetrated into the scar tissue were counted manually. For image analysis, c-Fos-positive (c-Fos+) nuclei from all sections was superimposed onto Molander's cytoarchitectonic maps of the rat thoracic and lumbosacral cord [57]. The expression of synapsin-1 was examined within lamina IX of the L1-L5 segments of the spinal cord using transverse sections and DAB staining. For the quantification of BDA tracing, we followed the methods reported previously [58,59]. The number of CST-positive axons at each distance from the lesion was divided by the number of CST-positive axons at the level of C1 for standardization.

Statistical analyses

For statistical analyses, one-way analyses of variance (one-way ANOVA) and Bonferroni *post hoc* tests were primarily employed to determine significance. Significance was determined using P-values, and the data are presented

as the means ± S.E.M. For the analysis of 5-HT immunostaining, data were analyzed with the Kruskal-Wallis H test. Behavioral data after re-transection were analyzed with t-tests.

Additional file

Additional file 1: Video Representative movies of the *detailed* kinematic *analysis of hindlimb motor performance* on a treadmill at the end of the experimental period. Plantar step walking with a BSS was not observed in control group animals (A). Limited plantar step walking with a BSS was observed in SM-345431 treatment group animals (B). Significantly enhanced plantar step walking with a BSS was observed in the combined treatment group animals. All animals in the combined treatment group continued plantar step walking with a BSS for at least 30 min (C).

Competing interests

H. Okano is a scientific consultant of San Bio, Inc; Eisai Co Ltd; and Daiichi Sankyo Co Ltd.
K. Kikuchi, A. Sano, M. Maeda, A. Kishino and T. Kimura are employed by Dainippon Sumitomo Pharma Co Ltd.

Authors' contributions

LZ and SK performed the experiments and wrote the manuscript. KK, AS, MM, SS, and MM performed the experiments. SK, AK, YT, ML, TK, HO and MM designed the study. All authors read and approved the final manuscript.

Acknowledgments

We thank Kiyokazu Iwata, Toshihiro Nagai and Takahiro Kondo for sample preparation and all members of the Okano laboratory for helpful discussions and support.
This work was supported by grants from the Project for the Realization of Regenerative Medicine from the Ministry of Education, Culture, Sports and Technology (MEXT) of Japan and the Research Center Network for the Realization of Regenerative Medicine to H.O. and M.N.; a grant for young investigators from MEXT to S.K.; a grant from the General Insurance Association of Japan to L.Z., S.K. and M.N. and the Funding Program for World-Leading Innovative R&D on Science and Technology (FIRST Program) to H.O.

Author details

[1]Department of Orthopedic Surgery, Keio University School of Medicine, 35 Shinanomachi, Shinjuku, Tokyo 160-8582, Japan. [2]Department of Physiology, Keio University School of Medicine, 35 Shinanomachi, Shinjuku, Tokyo 160-8582, Japan. [3]Department of Rehabilitation Medicine, Keio University School of Medicine, 35 Shinanomachi, Shinjuku, Tokyo 160-8582, Japan. [4]Department of Orthopedic Surgery, National Hospital Organization, Murayama Medical Center, 2-37-1 Gakuen, Musashimurayama, Tokyo 208-0011, Japan. [5]Dainippon Sumitomo Pharma Co. Ltd., 3-1-98 Kasugade-naka, Konohana-ku, Osaka 554-0022, Japan.

Received: 20 January 2014 Accepted: 12 February 2014
Published: 10 March 2014

References

1. Afshari FT, Kappagantula S, Fawcett JW: Extrinsic and intrinsic factors controlling axonal regeneration after spinal cord injury. *Expert Rev Mol Med* 2009, 11:1–19.
2. Chierzi S, Ratto GM, Verma P, Fawcett JW: The ability of axons to regenerate their growth cones depends on axonal type and age, and is regulated by calcium, cAMP and ERK. *Eur J Neurosci* 2005, 21(8):2051–2062.
3. Davies SJ, Goucher DR, Doller C, Silver J: Robust regeneration of adult sensory axons in degenerating white matter of the adult rat spinal cord. *J Neurosci* 1999, 19(14):5810–5822.
4. Silver J, Miller JH: Regeneration beyond the glial scar. *Nat Rev Neurosci* 2004, 5(2):146–156.
5. Filbin MT: Myelin-associated inhibitors of axonal regeneration in the adult mammalian CNS. *Nat Rev Neurosci* 2003, 4(9):703–713.
6. GrandPre T, Nakamura F, Vartanian T, Strittmatter SM: Identification of the Nogo inhibitor of axon regeneration as a Reticulon protein. *Nature* 2000, 403(6768):439–444.
7. He Z, Koprivica V: The nogo signaling pathway for regeneration block. *Annu Rev Neurosci* 2004, 27(1:341–368.
8. McKerracher L, David S, Jackson DL, Kottis V, Dunn RJ, Braun PE: Identification of myelin-associated glycoprotein as a major myelin-derived inhibitor of neurite growth. *Neuron* 1994, 13(4):805–811.
9. Wang KC, Koprivica V, Kim JA, *et al*: Oligodendrocyte-myelin glycoprotein is a Nogo receptor ligand that inhibits neurite outgrowth. *Nature* 2002, 417(6892):941–944.
10. Bradbury EJ, Moon LD, Popat RJ, *et al*: Chondroitinase ABC promotes functional recovery after spinal cord injury. *Nature* 2002, 416(6881):636–640.
11. McKeon RJ, Schreiber RC, Rudge JS, Silver J: Reduction of neurite outgrowth in a model of glial scarring following CNS injury is correlated with the expression of inhibitory molecules on reactive astrocytes. *J Neurosci* 1991, 11(11):3398–3411.
12. De Winter F, Holtmaat AJ, Verhaagen J: Neuropilin and class 3 semaphorins in nervous system regeneration. *Adv Exp Med Biol* 2002, 515:115–139.
13. Pasterkamp RJ, Giger RJ, Ruitenberg MJ, *et al*: Expression of the gene encoding the chemorepellent semaphorin III is induced in the fibroblast component of neural scar tissue formed following injuries of adult but not neonatal CNS. *Mol Cell Neurosci* 1999, 13(2):143–166.
14. Hata K, Fujitani M, Yasuda Y, *et al*: RGMa inhibition promotes axonal growth and recovery after spinal cord injury. *J Cell Biol* 2006, 173(1):47–58.
15. Schwab JM, Conrad S, Monnier PP, Julien S, Mueller BK, Schluesener HJ: Spinal cord injury-induced lesional expression of the repulsive guidance molecule (RGM). *Eur J Neurosci* 2005, 21(6):1569–1576.
16. Kim JE, Li S, GrandPre T, Qiu D, Strittmatter SM: Axon regeneration in young adult mice lacking Nogo-A/B. *Neuron* 2003, 38(2):187–199.
17. Simonen M, Pedersen V, Weinmann O, *et al*: Systemic deletion of the myelin-associated outgrowth inhibitor Nogo-A improves regenerative and plastic responses after spinal cord injury. *Neuron* 2003, 38(2):201–211.
18. Taniguchi M, Yuasa S, Fujisawa H, *et al*: Disruption of semaphorin III/D gene causes severe abnormality in peripheral nerve projection. *Neuron* 1997, 19(3):519–530.
19. Kikuchi K, Kishino A, Konishi O, *et al*: In vitro and in vivo characterization of a novel semaphorin 3A inhibitor, SM-216289 or xanthofulvin. *J Biol Chem* 2003, 278(44):42985–42991.
20. Kaneko S, Iwanami A, Nakamura M, *et al*: A selective Sema3A inhibitor enhances regenerative responses and functional recovery of the injured spinal cord. *Nat Med* 2006, 12(12):1380–1389.
21. García-Alías G, Barkhuysen S, Buckle M, Fawcett JW: Chondroitinase ABC treatment opens a window of opportunity for task-specific rehabilitation. *Nat Neurosci* 2009, 12(9):1145–1151.
22. Heng C, de Leon RD: Treadmill training enhances the recovery of normal stepping patterns in spinal cord contused rats. *Exp Neurol* 2009, 216(1):139–147.
23. Winchester P, McColl R, Querry R, *et al*: Changes in supraspinal activation patterns following robotic locomotor therapy in motor-incomplete spinal cord injury. *Neurorehabil Neural Repair* 2005, 19(4):313–324.
24. Courtine G, Gerasimenko Y, van den Brand R, *et al*: Transformation of nonfunctional spinal circuits into functional states after the loss of brain input. *Nat Neurosci* 2009, 12(10):1333–1342.
25. Barbeau H, Rossignol S: Recovery of locomotion after chronic spinalization in the adult cat. *Brain Res* 1987, 412(1):84–95.
26. Kubasak MD, Hedlund E, Roy RR, Carpenter EM, Edgerton VR, Phelps PE: L1 CAM expression is increased surrounding the lesion site in rats with complete spinal cord transection as neonates. *Exp Neurol* 2005, 194(2):363–375.
27. Ichiyama R, Gerasimenko Y, Zhong H, Roy R, Edgerton V: Hindlimb stepping movements in complete spinal rats induced by epidural spinal cord stimulation. *Neurosci Lett* 2005, 383(3):339–344.
28. Kubasak MD, Jindrich DL, Zhong H, *et al*: OEG implantation and step training enhance hindlimb-stepping ability in adult spinal transected rats. *Brain* 2007, 131(1):264–276.
29. Acevedo LM, Barillas S, Weis SM, Gothert JR, Cheresh DA: Semaphorin 3A suppresses VEGF-mediated angiogenesis yet acts as a vascular permeability factor. *Blood* 2008, 111(5):2674–2680.

30. Kolodkin AL, VD L, *et al*: **neuropilin is a semaphorin III receptor.** *Cell* 1997, **90**:753–762.
31. Guizarsahagun G, Ibarra A, Espitia A, Martinez A, Madrazo I, Francobourland R: **Glutathione monoethyl ester improves functional recovery, enhances neuron survival, and stabilizes spinal cord blood flow after spinal cord injury in rats.** *Neuroscience* 2005, **130**(3):639–649.
32. Imperato-Kalmar EL, McKinney RA, Schnell L, Rubin BP, Schwab ME: **Local changes in vascular architecture following partial spinal cord lesion in the rat.** *Exp Neurol* 1997, **145**(2 Pt 1):322–328.
33. Loy DN, Crawford CH, Darnall JB, Burke DA, Onifer SM, Whittemore SR: **Temporal progression of angiogenesis and basal lamina deposition after contusive spinal cord injury in the adult rat.** *J Comp Neurol* 2002, **445**(4):308–324.
34. Casella GTB, Marcillo A, Bunge MB, Wood PM: **New vascular tissue rapidly replaces neural parenchyma and vessels destroyed by a contusion injury to the Rat spinal cord.** *Exp Neurol* 2002, **173**(1):63–76.
35. Kitamura K, Iwanami A, Nakamura M, *et al*: **Hepatocyte growth factor promotes endogenous repair and functional recovery after spinal cord injury.** *J Neurosci Res* 2007, **85**(11):2332–2342.
36. Piaton G, Aigrot MS, Williams A, *et al*: **Class 3 semaphorins influence oligodendrocyte precursor recruitment and remyelination in adult central nervous system.** *Brain* 2011, **134**(4):1156–1167.
37. Kiehn O: **Locomotor circuits in the mammalian spinal cord.** *Annu Rev Neurosci* 2006, **29**:279–306.
38. Kiehn O, Kjaerulff O: **Distribution of central pattern generators for rhythmic motor outputs in the spinal cord of limbed vertebrates.** *Ann N Y Acad Sci* 1998, **860**:110–129.
39. Gulino R, Dimartino M, Casabona A, Lombardo SA, Perciavalle V: **Synaptic plasticity modulates the spontaneous recovery of locomotion after spinal cord hemisection.** *Neurosci Res* 2007, **57**(1):148–156.
40. Ying Z, Roy R, Edgerton V, Gomezpinilla F: **Exercise restores levels of neurotrophins and synaptic plasticity following spinal cord injury.** *Exp Neurol* 2005, **193**(2):411–419.
41. Ahn SN, Guu JJ, Tobin AJ, Edgerton VR, Tillakaratne NJ: **Use of c-fos to identify activity-dependent spinal neurons after stepping in intact adult rats.** *Spinal Cord* 2006, **44**(9):547–559.
42. Huang A, Noga B, Carr P, Fedirchuk B, Jordan L: **Spinal cholinergic neurons activated during locomotion: localization and electrophysiological characterization.** *J Neurophysiol* 2000, **83**:3537–3547.
43. Ichiyama RM, Courtine G, Gerasimenko YP, *et al*: **Step training reinforces specific spinal locomotor circuitry in adult spinal rats.** *J Neurosci* 2008, **28**(29):7370–7375.
44. de Leon RD, Acosta CN: **Effect of robotic-assisted treadmill training and chronic quipazine treatment on hindlimb stepping in spinally transected rats.** *J Neurotrauma* 2006, **23**(7):1147–1163.
45. Maier IC, Ichiyama RM, Courtine G, *et al*: **Differential effects of anti-Nogo-A antibody treatment and treadmill training in rats with incomplete spinal cord injury.** *Brain* 2009, **132**(6):1426–1440.
46. Bareyre FM, Kerschensteiner M, Raineteau O, Mettenleiter TC, Weinmann O, Schwab ME: **The injured spinal cord spontaneously forms a new intraspinal circuit in adult rats.** *Nat Neurosci* 2004, **7**(3):269–277.
47. Raineteau O, Schwab ME: **Plasticity of motor systems after incomplete spinal cord injury.** *Nat Rev Neurosci* 2001, **2**:263–273.
48. Courtine G, Song B, Roy RR, *et al*: **Recovery of supraspinal control of stepping via indirect propriospinal relay connections after spinal cord injury.** *Nat Med* 2008, **14**(1):69–74.
49. Dunlop SA: **Activity-dependent plasticity: implications for recovery after spinal cord injury.** *Trends Neurosci* 2008, **31**(8):410–418.
50. Kiehn O, Kjaerulff O: **Spatiotemporal characteristics of 5-HT and dopamine-induced rhythmic hindlimb activity in the in vitro neonatal rat.** *J Neurophysiol* 1996, **75**(4):1472–1482.
51. Feraboli-Lohnherr D, Orsal D, Yakovleff A, Gimenez y Ribotta M, Privat A: **Recovery of locomotor activity in the adult chronic spinal rat after sublesional transplantation of embryonic nervous cells: specific role of serotonergic neurons.** *Exp Brain Res* 1997, **113**(3):443–454.
52. Edgerton VR, Tillakaratne NJK, Bigbee AJ, de Leon RD, Roy RR: **Plasticity of the spinal neural circuitry after injury.** *Annu Rev Neurosci* 2004, **27**(1):145–167.
53. Cote MP, Menard A, Gossard JP: **Spinal cats on the treadmill: changes in load pathways.** *J Neurosci* 2003, **23**(7):2789–2796.
54. Nave K-A: **Myelination and support of axonal integrity by glia.** *Nature* 2010, **468**(7321):244–252.
55. Nessler JA, Timoszyk W, Merlo M, *et al*: **A robotic device for studying rodent locomotion after spinal cord injury.** *IEEE Trans Neural Syst Rehabil Eng* 2005, **13**(4):497–506.
56. Timoszyk W, Nessler J, Acosta C, *et al*: **Hindlimb loading determines stepping quantity and quality following spinal cord transection.** *Brain Res* 2005, **1050**(1–2):180–189.
57. Molander C, Xu Q, Grant G: **The cytoarchitectonic organization of the spinal cord in the rat. I. The lower thoracic and lumbosacral cord.** *J Comp Neurol* 1984, **230**(1):133–141.
58. Wang D, Ichiyama RM, Zhao R, Andrews MR, Fawcett JW: **Chondroitinase combined with rehabilitation promotes recovery of forelimb function in rats with chronic spinal cord injury.** *J Neurosci* 2011, **31**(25):9332–9344.
59. Zheng B, Ho C, Li S, Keirstead H, Steward O, Tessier-Lavigne M: **Lack of enhanced spinal regeneration in Nogo-deficient mice.** *Neuron* 2003, **38**(2):213–224.

doi:10.1186/1756-6606-7-14
Cite this article as: Zhang *et al.*: Rewiring of regenerated axons by combining treadmill training with semaphorin3A inhibition. *Molecular Brain* 2014 **7**:14.